UNIVERSIDADE FEDERAL DO CEARÁ

CENTRO DE TECNOLOGIA

DEPARTAMENTO DE ENGENHARIA DE TELEINFORMÁTICA

PROGRAMA DE PÓS-GRADUAÇÃO EM ENGENHARIA DE TELEINFORMÁTICA

DOUTORADO EM ENGENHARIA DE TELEINFORMÁTICA

ITALO PEREIRA BEZERRA

PHASE SPACE DISPLACEMENT, QUADRATURE SQUEEZING AND TEMPERATURE ESTIMATION FROM THE FOCK DISTRIBUTION FOR 1-MODE GAUSSIAN STATES

FORTALEZA

2023

ITALO PEREIRA BEZERRA

PHASE SPACE DISPLACEMENT, QUADRATURE SQUEEZING AND TEMPERATURE ESTIMATION FROM THE FOCK DISTRIBUTION FOR 1-MODE GAUSSIAN STATES

Thesis submitted to the Programa de Pós-Graduação em Engenharia de Teleinformática of the Centro de Tecnologia of the Universidade Federal do Ceará, as a partial requirement for obtaining the title of Doctor in Teleinformatics Engineering. Concentration Area: Applied Electromagnetism

Advisor: Prof. Hilma H. Macedo de Vasconcelos

Co-advisor: Dr. Scott Charles Glancy

FORTALEZA

2023

Dados Internacionais de Catalogação na Publicação
Universidade Federal do Ceará
Sistema de Bibliotecas
Gerada automaticamente pelo módulo Catalog, mediante os dados fornecidos pelo(a) autor(a)

B469p Bezerra, Italo Pereira.
Phase Space Displacement, Quadrature Squeezing and Temperature Estimation from the Fock Distribution for 1-Mode Gaussian States / Italo Pereira Bezerra. – 2023.
70 f. : il. color.

Tese (doutorado) – Universidade Federal do Ceará, Centro de Tecnologia, Programa de Pós-Graduação em Engenharia de Teleinformática, Fortaleza, 2023.
Orientação: Profa. Dra. Hilma H. Macedo de Vasconcelos.
Coorientação: Prof. Dr. Scott C. Glancy.

1. Gaussian states. 2. Squeezing. 3. Phase space. 4. Quadratures. 5. Wigner function. I. Título.
CDD 621.38

ITALO PEREIRA BEZERRA

PHASE SPACE DISPLACEMENT, QUADRATURE SQUEEZING AND TEMPERATURE ESTIMATION FROM THE FOCK DISTRIBUTION FOR 1-MODE GAUSSIAN STATES

Thesis submitted to the Programa de Pós-Graduação em Engenharia de Teleinformática of the Centro de Tecnologia of the Universidade Federal do Ceará, as a partial requirement for obtaining the title of Doctor in Teleinformatics Engineering. Concentration Area: Applied Electromagnetism

Approved on: August 25th, 2023

EXAMINATION BOARD

Prof. Hilma H. Macedo de Vasconcelos
(Advisor)
Universidade Federal do Ceará (UFC)

Dr. Scott Charles Glancy (Co-advisor)
National Institute of Standards and Technology
(NIST)

Prof. Daniel Felinto Pires Barbosa
Universidade Federal de Pernambuco (UFPE)

Prof. Liliana Sanz de la Torre
Universidade Federal de Uberlândia (UFU)

Prof. Rubens Viana Ramos
Universidade Federal do Ceará (UFC)

To my wife Elaine and my son Daniel, essential company in this journey

ACKNOWLEDGEMENTS

I'm very grateful to my supervisors Dr. Hilma Vasconcelos and Dr. Scott Glancy for all the support, patience and opportunities in this long road. Special thanks also go to my professors Dr. Rubens Ramos and Dr. João Batista for support and advice. Thanks to my colleagues at GIQ for the support and to Daniel Slitcher and Hannah Knaack from NIST for the discussions and suggestions. Finally, I want to say thanks to the Programa de Pós-Graduação em Engenharia de Teleinformática (PPGETI), to the Universidade Estadual do Ceará (UECE) for the financial support and to the National Institute of Standards and Technology (NIST) for the opportunity of being there and all the support when visiting the institute, including the financial support.

ABSTRACT

We present a method to estimate the amount of displacement, squeezing and temperature of a single-mode harmonic oscillator state based on both the weighted least squares and maximum likelihood estimators applied to measured Fock state populations and fluorescence measurements. Displacement, squeezing and temperature, or equivalently the mean of the quadratures and its variances, are essential state parameters used in quantum computation and various communication and sensing protocols. They are often measured with homodyne-style detection, which requires a phase reference such as a local oscillator. Our method allows estimation without a phase reference, by using for example a photon-number-resolving detector. To evaluate the performance of our estimator, we simulated experiments with different values of displacement, squeezing, phase and temperature. First we simulate Fock population measurement experiments. From 10,000 Fock measurement events we produced estimates for states whose fidelities to the true state are greater than 99.99% for small squeezing ($r < 1.0$), and for high squeezing ($r = 2.5$) we obtain fidelities greater than 99.9%. We also report confidence intervals and their coverage probabilities, mean squared error and their coverage probabilities. We also simulate fluorescence measurement experiments for different motional states of a trapped ion. Jointly fitting datasets for different relative phases helped to decrease significantly the uncertainty on the estimates. Based on the analysis of real data we proposed a correction to the model that describes the probability of measuring the ion on the spin down state.

Keywords: Gaussian states. Temperature. Squeezing. Estimate. Fidelity.

LIST OF FIGURES

LIST OF TABLES

LIST OF SYMBOLS

m	mass of the classical harmonic oscillator
H	Hamiltonian of the harmonic oscillator
$\mathbf{p}$	linear moment
$\mathbf{q}$	position
ω	angular frequency of the harmonic oscillator
$\hat{\mathbf{p}}$	linear moment operator
$\hat{\mathbf{q}}$	position operator
$\hat{a}^\dagger$	creation operator
$\hat{a}$	anihilation operator
$\hat{p}$	quadrature operator p
$\hat{q}$	quadrature operator q
Ψ	Condutor de neutro
$\hat{\rho}$	density operator
W	Wigner function
W_0	Wigner function for vacuum state
W_n	Wigner function for Fock state $\|n\rangle$
H_n	Hermite polynomial of order n
L_n	Laguerre polynomial of order n
$\hat{D}(\alpha)$	displacement operator
α	complex displacement in the phase space
θ	displacement phase
$P(n)$	probability function of finding the state in the Fock number n
$\hat{S}(\zeta)$	squeezing operator
ζ	squeezing factor
r	amount of squeezing
ϕ	squeezing phase

$P(n\|\alpha)$	probability function of finding the displaced state with displacement α in the Fock number n
$\hat{a}_s^\dagger$	squeezed creation operator
$\hat{a}_s$	squeezed anihilation operator
$\hat{\rho}_{th}$	density operator for thermal state
$\bar{n}$	mean Fock number
X	quadrature vector
Σ	covariance matrix
d	vector of means
$\hat{\rho}_s$	density operator for squeezed thermal state
V_p	variance of p
V_q	variance of q
$\mathbf{H}_{mn}^R$	2-dimensional Hermite polynomial
M	model function
N_d	number of points of a dataset
w	weights associated to the data
σ	standard deviation
N	number of times an experiment is repeated.
k_i	number of detections in an experiment
$\Delta(...)$	weighted sum of squared residuals
f_n	relative frequency of measurements k_i/N
p	binomial success probability
$Beta(\nu, \eta)$	Beta function
ν, η	shape parameters of a beta distribution
$F(\rho_1, \rho_2)$	Fidelity between ρ_1 and ρ_2
Ξ, Λ	elements of fidelity function for gaussian states
$\mathbf{f}$	data vector
C_i, C_j	confidence interval limits

N_B	number of bootstrap samples
β	parameter associated to the size of the conf. interval. The level of confidence if given by $100(1-2\beta)$
$\boldsymbol{\Theta}$	estimator of a parameter Θ
B	Bias
$\hat{\rho}_f$	density operator of final state
$\mathbf{L}$	log-likelihood function

CONTENTS

1 INTRODUCTION

Estimating the state of a quantum system is an important tool for quantum information processing. It allows one, for example, to quantify the accuracy of prepared states, diagnose errors in the state, and estimate properties such as entanglement measures. State reconstruction is done in two steps: data extraction from the experiment and statistical estimation. For continuous variable systems, such as harmonic oscillators, the first is usually accomplished by using balanced homodyne detection to measure quadratures (Lvovsky and Raymer 2009; Mallet *et al.* 2011; Raffaelli *et al.* 2018). Sets of quadratures measured at different phases can be used to reconstruct the system's Wigner function by using a numerical inverse Radon transform (Smithey *et al.* 1993), or one may reconstruct its Fock-basis density matrix by maximizing the likelihood function (Řeháček *et al.* 2007) or by other techniques. Another strategy for state estimation is to apply a displacement operator followed by Fock-state parity measurement, as done in (Leibfried *et al.* 1996) and (Hofheinz *et al.* 2009). The homodyne-detection and the displacement-and-Fock-parity strategies require a phase reference to serve as a local oscillator and to apply the displacement, respectively. However, in some systems, phase-sensitive detection is not easily available; examples are integrated optical circuits that use photon-number resolving detectors (Sahin *et al.* 2013; Höpker *et al.* 2019; Arrazola *et al.* 2021) and trapped ions whose motional Fock states are measured by coupling to the ions' qubit states (Meekhof *et al.* 1996; Burd *et al.* 2019; Myerson *et al.* 2008). In such systems, one would still like to estimate those features of a quantum state that are phase-independent.

We focus on single-mode, Gaussian states, which we call "squeezed displaced thermal states". Squeezed states have been studied for applications such as measurement noise reduction (Acernese *et al.* 2019; Tse *et al.* 2019), as generators of entanglement in continuous variable quantum teleportation (Furusawa *et al.* 1998), and as resource states for quantum computation (Gottesman *et al.* 2001). Some applications of coherent states are optical quantum computation (Ralph *et al.* 2003) and quantum metrology (Joo *et al.* 2011; Wineland and Leibfried 2011). We present here methods for inferring a system's displacement, squeezing and temperature based on Fock state measurements. First we do it by minimizing the weighted squared errors between the probabilities of measuring each Fock number and the frequency of observing that Fock number. Then, in a second part of the work, we apply both least squares minimization and log-likelihood maximization but now using the frequency of observing fluorescence data from a single trapped ion. Although this data is modeled by the probability of observing the ion in the spin down state,

it depends on the Fock population associated to the ion's motional state. Because we measure only Fock populations, we do not have access to the phase information. The first method can be applied to any type of quantum oscillator such as superconducting resonators, single trapped ions, and photons. From 10,000 measurements, we obtained fidelities between the true state and the estimated state $> 99.99\%$ for small squeezing ($r < 1.0$). Even for high squeezing ($r = 2.5$) the estimate's fidelity with the true state is greater than 99.9%. The second method can be applied to single-trapped ion data, allowing the estimation of the ion's motional state parameters.

The thesis is organized as follows: In the second chapter, we present an introduction to one mode Gaussian states including its Fock population probabilities. In the third chapter, we present the results for squeezed displaced thermal states from simulated experiments analysis, for different values of total number of measurements, temperature and squeezing including confidence intervals and bias correction. In chapter four, we present the results for a more general state, the squeezed displaced thermal state, by analysing simulated data from blue sideband (BSB) measurements for a trapped ion. In the same chapter, our estimator is applied to real data and analysed, leading to a proposal of a new model for this kind of measurements and its analysis. In chapter five, we present a brief review of the most important results.

2 GAUSSIAN STATES

Gaussian states plays a major role in quantum information with continuous variables. They are suitable to describe many bosonic systems such as trapped ions, which has been intensively studied in the last 40 years.

A system of N bosonic modes can be described by a set of N quantum harmonic oscillators. Classically, a particle with mass m allowed to move in a direction $\mathbf{q}$ with momentum $\mathbf{p}$ and subjected to a parabolic potential has its Hamiltonian written as

$$H = \frac{\mathbf{p}^2}{2m} + \frac{m\omega^2\mathbf{q}}{2}, \tag{2.1}$$

where $\mathbf{q}$ and $\mathbf{p}$ are the position and momentum variables. The transition to the quantum domain is obtained by replacing $\mathbf{q}$ and $\mathbf{p}$ by a set of conjugate operators $\hat{\mathbf{q}}$ and $\hat{\mathbf{p}}$ such that the Hamiltonian operator $\hat{H}$ is given by

$$\hat{H} = \frac{\hat{\mathbf{p}}^2}{2m} + \frac{m\omega^2\hat{\mathbf{q}}}{2}. \tag{2.2}$$

Now, $\hat{\mathbf{q}}$ and $\hat{\mathbf{p}}$ are the position and momentum operators. The eigenvalue E and the eigenfunction ψ associated to $\hat{H}$ can be obtained from the equation $\hat{H}\psi(\mathbf{q}) = E\psi(\mathbf{q})$, the Schrodinger equation. This Hamiltonian can be rewritten in terms of two non-hermitian operators $\hat{a}$ and $\hat{a}^\dagger$, the annihilation and creation operators, given by

$$\hat{a} = \frac{m\omega\,\hat{\mathbf{q}} + i\hat{\mathbf{p}}}{\sqrt{2m\omega\hbar}}, \quad \text{and} \quad \hat{a}^\dagger = \frac{m\omega\,\hat{\mathbf{q}} - i\hat{\mathbf{p}}}{\sqrt{2m\omega\hbar}}, \tag{2.3}$$

resulting in the known expression for the Hamiltonian of any single-mode quantum harmonic oscillator

$$\hat{H} = \hbar\omega\left(\hat{a}^\dagger\hat{a} + \frac{1}{2}\right), \tag{2.4}$$

with eigenvalues $E_n = \hbar\omega\left(n + \frac{1}{2}\right)$ and eigenfunctions ψ_n, where n is integer. The eigenstates of the Hamiltonian operator are given by $|n\rangle$, the Fock states, and form an orthonormal basis in the Hilbert space. It is possible to write $\hat{a}$ and $\hat{a}^\dagger$ in terms of dimensionless position and momentum operators

$$\hat{q} = \frac{(\hat{a} + \hat{a}^\dagger)}{\sqrt{2}}, \quad \text{and} \quad \hat{p} = \frac{(\hat{a} - \hat{a}^\dagger)}{i\sqrt{2}}, \tag{2.5}$$

the quadrature operators. These operators are Hermitian and have a continuous spectra of eigenvalues given by

$$\hat{q}\,|q\rangle = q\,|q\rangle, \quad \text{and} \quad \hat{p}\,|p\rangle = p\,|p\rangle, \tag{2.6}$$

and obey the commutation relation $[\hat{q},\hat{p}] = i$. By using the properties of the annihilation operator it is possible to obtain the eigenfunction for $|0\rangle$, as a function of the eigenvalues of the quadrature $\hat{q}$. For that, we use the definition of the annihilation operator applied to the ground state eigenfunction resulting in the differential equation $\hat{a}\psi_0 + \frac{d}{dq}\psi_0 = 0$. The resulting eigenfunction is given by

$$\psi_0(q) = \pi^{-1/4} e^{-q^2/2}, \tag{2.7}$$

a Gaussian function of q. The eigenfunction of $\hat{p}$ can be obtained by a Fourier transform of $\psi_0(q)$ resulting in the eigenfunction

$$\psi_0(p) = \pi^{-1/4} e^{-p^2/2}. \tag{2.8}$$

It is interesting to note that both functions are Gaussian. Also, both looks like marginal distributions of a joint distribution of q and p. In fact, there is a more appropriate representation of a quantum state when it can be described by the quadrature operators. It is called the Wigner function and is defined as

$$W(q,p) = \frac{1}{2\pi}\int_{-\infty}^{+\infty} \langle q - s/2|\,\hat{\rho}\,|q + s/2\rangle\, e^{ips} ds, \tag{2.9}$$

where $\hat{\rho}$ is the density operator. For the vacuum state $\hat{\rho} = |0\rangle\langle 0|$ and its Wigner function can be obtained by

$$\begin{aligned}
W_0(q,p) &= \frac{1}{2\pi}\int_{-\infty}^{+\infty} \langle q - s/2|0\rangle\langle 0|q - s/2\rangle\, e^{ips} ds \\
&= \frac{1}{2\pi}\int_{-\infty}^{+\infty} \psi_0^*(q + s/2)\psi_0(q - s/2) e^{ips} ds \\
&= \frac{\pi^{-1/2}}{2\pi}\int_{-\infty}^{+\infty} \exp\left[-(q - s/2)^2/2 - (q + s/2)^2/2 + ips\right] ds \\
&= \frac{\pi^{-1/2}}{2\pi}\int_{-\infty}^{+\infty} \exp\left[-q^2 - p^2\right] \exp\left[-(s/2 - ip)^2\right] ds \\
&= \frac{\pi^{-1/2} e^{-q^2-p^2}}{2\pi}\int_{-\infty}^{+\infty} e^{-(s/2-ip)^2} ds \\
&= \frac{1}{\pi} e^{-q^2-p^2}.
\end{aligned} \tag{2.10}$$

That is a 2-dimensional Gaussian distribution of q and p. Such states whose Wigner functions are Gaussian are called Gaussian States. For Fock states with $n > 0$, the Wigner function $W_n(q,p)$ can be obtained by replacing $\hat{\rho} = |n\rangle\langle n|$ in Eq. (2.9):

$$\begin{aligned}
W_n(q,p) &= \frac{1}{2\pi}\int_{-\infty}^{+\infty} \langle q - s/2|n\rangle\langle n|q - s/2\rangle\, e^{ips} ds \\
&= \frac{1}{2\pi}\int_{-\infty}^{+\infty} \psi_n^*(q + s/2)\psi_n(q - s/2) e^{ips} ds,
\end{aligned} \tag{2.11}$$

where $\psi_n(q)$ is the eigenfunction of $|n\rangle$ and is given by

$$\psi_n(q) = \frac{H_n(q)}{\sqrt{2^n n!}\sqrt{\pi}}\, e^{-q^2/2}, \tag{2.12}$$

where $H_n(q)$ is the Hermite polynomial of order n. The resulting Wigner function $W_n(q,p)$ is given by

$$W_n(q,p) = \frac{(-1)^n}{\pi} e^{-q^2+p^2} L_n(2q^2+2p^2), \tag{2.13}$$

and L_n are the Laguerre polynomials. Figure 1 shows the Wigner functions for $n=0$, $n=1$ and $n=2$. The first one is a 2-dimensional Gaussian distribution centered on the origin. For $n=1$ and $n=2$ it is interesting to note that the function presents negative values indicating non-classical behaviour of the states. Among all possible quantum states described by the continuum spectra of the quadrature operators $\hat{q}$ and $\hat{p}$, we focus in this work in those whose $W(q,p)$ is Gaussian.

Since $|0\rangle$ has a Gaussian representation in the phase space, any operation on the mean of the quadratures and on its covariance matrix will also result in a quantum state with a Gaussian distribution in the phase space. For example, displacing the center of the Gaussian to a point (q_0, p_0) results in a displaced Gaussian where $\alpha = q_0 + ip_0$ is the displacement in the phase space. It is called the displaced state and it is the eigenstate of the annihilation operator, $\hat{a}_k |\alpha\rangle = \alpha |\alpha\rangle$, and can be obtained from displacing the vacuum state $|0\rangle$ by

$$\hat{D}(\alpha)|\alpha\rangle = e^{\alpha\hat{a}^\dagger - \alpha^*\hat{a}}|\alpha\rangle. \tag{2.14}$$

In the number states basis the displaced state can be written as

$$|\alpha\rangle = e^{-\frac{1}{2}|\alpha|^2} \sum_{n=0}^{\infty} \frac{\alpha^n}{\sqrt{n!}} |n\rangle. \tag{2.15}$$

The probability of finding $|\alpha\rangle$ in a Fock number n is given by

$$P(n|\alpha) = |\langle n|\alpha\rangle|^2 = e^{-|\alpha|^2} \frac{|\alpha|^2}{n!}. \tag{2.16}$$

It is interesting to note that although the displacement can be written as $\alpha = |\alpha| e^{i\theta}$, where θ is its argument, the probability function $P(n)$ depends only on its amount of displacement $|\alpha|$.

Another important Gaussian state can be obtained by applying the operator

$$\hat{S} = \exp\left[\frac{\zeta \hat{a}^2}{2} - \frac{\zeta^* (\hat{a}^\dagger)^2}{2}\right] \tag{2.17}$$

to $|0\rangle$, resulting in the squeezed state

$$|\zeta\rangle = \hat{S}(\zeta)|0\rangle. \tag{2.18}$$

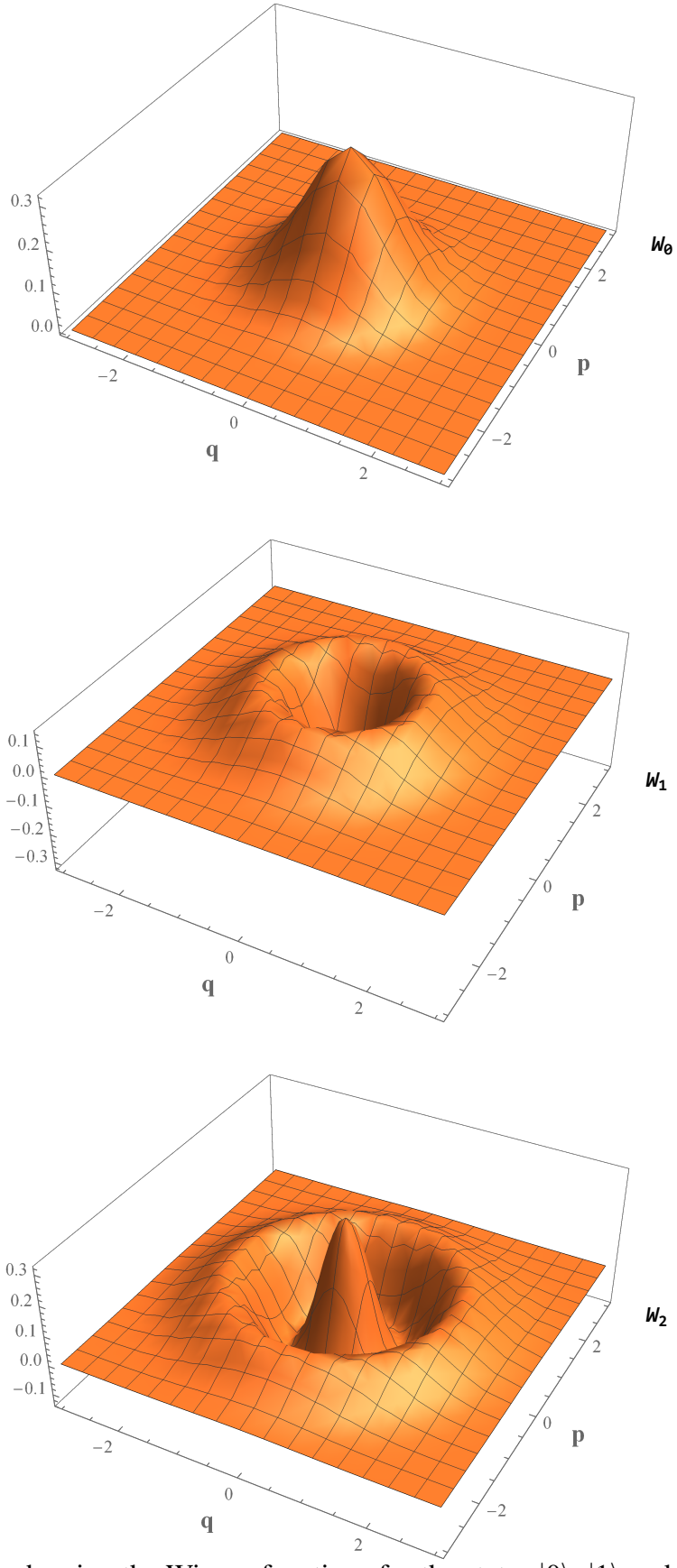

Figure 1 – Graphs showing the Wigner functions for the states $|0\rangle$, $|1\rangle$ and $|2\rangle$. Only the first presents 2-dimensional Gaussian shape.

$\hat{S}$ is the squeezing operator, $\zeta = re^{-i\phi}$ is the squeezing parameter, r is the amount of squeezing applied and ϕ is the squeezing phase. The operators $\hat{a}$ and $\hat{a}^\dagger$ transforms under a squeezing operation according to

$$\begin{aligned} \hat{a}_s &= \hat{S}\hat{a}\hat{S}^\dagger, \\ \hat{a}_s &= \hat{a}\cosh r + \hat{a}^\dagger e^{i\phi}\sinh r, \end{aligned} \tag{2.19}$$

and

$$\begin{aligned} \hat{a}_s^\dagger &= \hat{S}\hat{a}^\dagger\hat{S}^\dagger, \\ \hat{a}_s^\dagger &= \hat{a}^\dagger\cosh r + \hat{a}e^{-i\phi}\sinh r, \end{aligned} \tag{2.20}$$

Consequently, rewriting equations (2.5) in its squeezed form for $\phi = 0$, we get

$$\begin{aligned} \hat{q}_s &= \frac{(\hat{a}_s + \hat{a}_s^\dagger)}{\sqrt{2}} \\ \hat{q}_s &= \frac{(\hat{a} + \hat{a}^\dagger)(\cosh r + \sinh r)}{\sqrt{2}} \\ \hat{q}_s &= \hat{q}e^r. \end{aligned} \tag{2.21}$$

Doing the same for the quadrature $\hat{p}$ results in the squeezed quadrature $\hat{p}_s = \hat{p}e^{-r}$. It shows that when the quadratures are squeezed by an amount r, the eigenvalues of the quadratures are enlarged in one direction and squeezed in the other direction. Consequently, the Wigner function for a squeezed state can be obtained from the distribution for the vacuum state by simply transforming its coordinates like

$$W_s(q,p) = W_0(qe^r, qe^{-r}). \tag{2.22}$$

The effect of the squeezing operator can be seen in Figure 2. The bigger the value of r, the more the Gaussian state is squeezed towards the chosen direction.

The Fock population of a squeezed state can be obtained from $P(n|\zeta) = |\langle n|\zeta\rangle|^2 = |\langle n|\hat{S}(\zeta)|0\rangle|^2$. The resulting expression is given by

$$P(2n|r) = \binom{2n}{n}\frac{1}{\cosh r}\left(\frac{1}{2}\tanh r\right)^{2n}. \tag{2.23}$$

That is zero for odd values of n, and $P(n|\zeta)$ does not depend on ϕ. Figure 3 shows three Fock populations for pure squeezed states for different values of r. The bigger the r, the bigger the size of the Fock population.

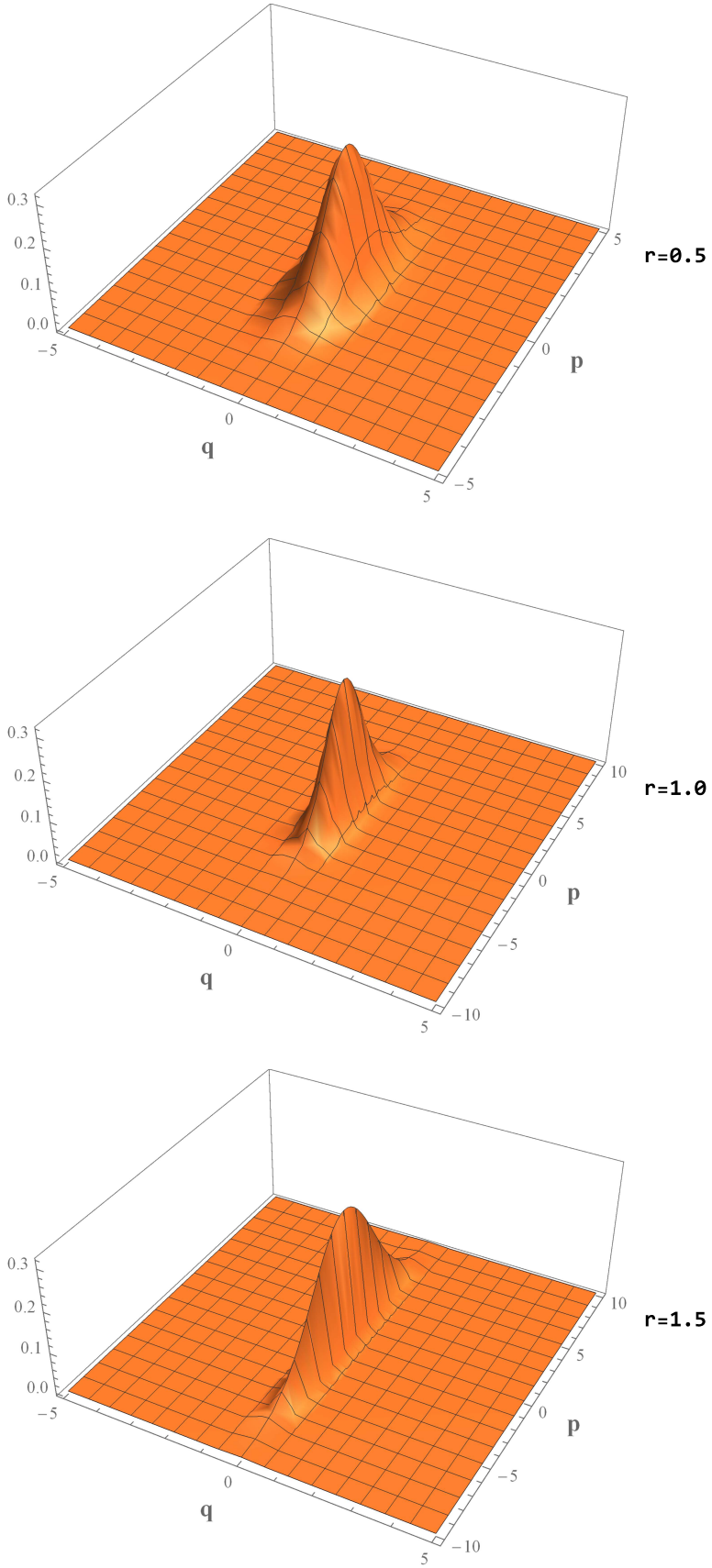

Figure 2 – Graphs showing the Wigner function for squeezed states with three different values of r. The squeezing phase ϕ is set to zero.

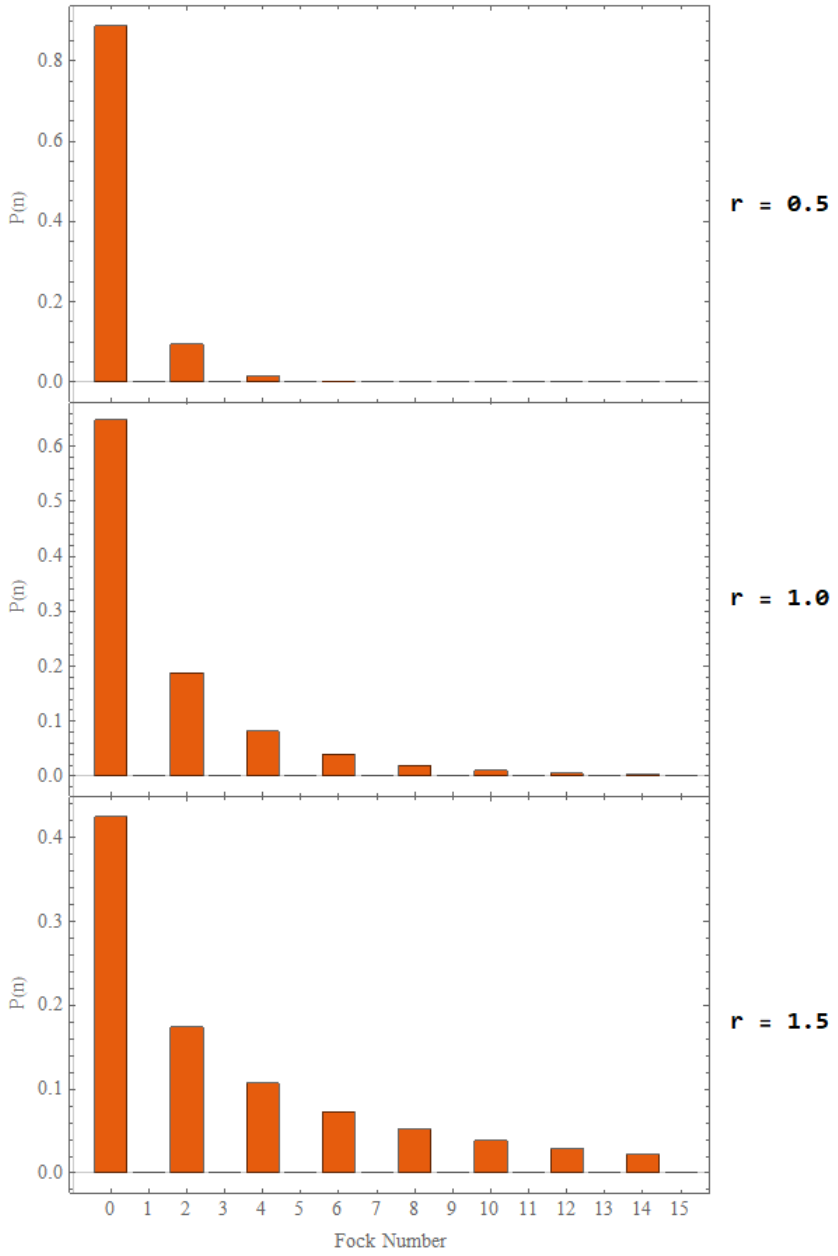

Figure 3 – Graphs showing the Fock populations for squeezed states with three different values of r. The squeezing phase ϕ is set to zero.

Another relevant set of 1-mode Gaussian states can be obtained from displacing or squeezing thermal states (or applying both operators in any order). These states are given by the density operator

$$\hat{\rho}_{th} = \sum_n \frac{\bar{n}^n}{(\bar{n}+1)^{n+1}} |n\rangle \langle n| . \tag{2.24}$$

Their Wigner functions can be obtained by using the definition

$$\begin{aligned}
W_{th}(q,p) &= \frac{1}{2\pi}\int_{-\infty}^{+\infty} \langle q-s/2|\, \hat{\rho}_{th}\, |q+s/2\rangle\, e^{ips} ds \\
&= \frac{1}{2\pi}\int_{-\infty}^{+\infty} \sum_n \frac{\bar{n}^n}{(\bar{n}+1)^{n+1}} \langle q-s/2|n\rangle \langle n|q-s/2\rangle\, e^{ips} ds \\
&= \frac{1}{2\pi}\sum_n \frac{\bar{n}^n}{(\bar{n}+1)^{n+1}} \int_{-\infty}^{+\infty} \langle q-s/2|n\rangle \langle n|q-s/2\rangle\, e^{ips} ds \\
&= \sum_n \frac{\bar{n}^n}{(\bar{n}+1)^{n+1}} W_n(q,p) \\
&= \sum_n \frac{\bar{n}^n}{(\bar{n}+1)^{n+1}} \frac{(-1)^n}{\pi} e^{-q^2-p^2} L_n(2q^2+2p^2) \\
&= \sum_n \frac{(-\bar{n})^n}{\pi(\bar{n}+1)^{n+1}} e^{-q^2-p^2} L_n(2q^2+2p^2) \\
&= \sum_{n=0}^{\infty} \frac{(-\bar{n})^n}{\pi(\bar{n}+1)^{n+1}} e^{-z/2} L_n(z) \\
&= \frac{e^{-z/2}}{\pi(\bar{n}+1)} \sum_n t^n L_n(z),
\end{aligned} \tag{2.25}$$

where $z = 2q^2 + 2p^2$ and $t = [(-\bar{n})/(\bar{n}+1)]^n$. Using the generating function for Laguerre polynomials

$$\sum_{n=0}^{\infty} t^n L_n(z) = \frac{1}{1-t} e^{-tz/(1-t)}, \tag{2.26}$$

the resulting Wigner function becomes

$$W_{th}(q,p) = \frac{1}{\pi(2\bar{n}+1)} e^{-(q^2+p^2)/(2\bar{n}+1)}, \tag{2.27}$$

and that is a Gaussian state.

All 1-mode Gaussian states obtained from both vacuum and thermal states have a bivariate Gaussian distribution that is characterized by the the first and second central statistical moments only. It means that the function is completely determined by its mean and its covariance matrix and has the general form

$$W(q,p) = \frac{1}{2\pi|\Sigma|^{-1}} \exp\left[-\frac{1}{2}(X-d)^T \Sigma^{-1} (X-d)\right], \tag{2.28}$$

where $\hat{X} = (\hat{q}, \hat{p})^{\mathrm{T}}$ is the quadrature operators vector, $X = (q, p)^{\mathrm{T}}$ the vector of eigenvalues and d is given by the expectation of $\hat{X}$

$$E[\hat{X}] = \langle \hat{X} \rangle = \mathrm{Tr}(\hat{X}\hat{\rho}) = (q_0, p_0)^T = d. \tag{2.29}$$

d is known as the first central moment. Σ, the second central moment, is the 2×2 covariance matrix of the Gaussian distribution. Its diagonal elements are the variances of the quadratures:

$$\begin{aligned} \Sigma_{ii} &= E[(\hat{X}_i - d_i)^2] \\ &= E[(\hat{X}_i^2 + d_i^2 - 2\hat{X}_i d_i)] \\ &= E[\hat{X}_i^2] + E[\hat{X}_i]^2 - 2d_i E[\hat{X}_i] \\ &= E[\hat{X}_i^2] - E[\hat{X}_i]^2. \end{aligned} \tag{2.30}$$

The off-diagonal elements, Σ_{ij}, are the covariance between the quadratures:

$$\begin{aligned} \Sigma_{ij} &= E[(\hat{X}_i - d_i)(\hat{X}_j - d_j)] \\ &= E[\hat{X}_i\hat{X}_j - d_i\hat{X}_j - d_j\hat{X}_i + d_i d_j] \\ &= E[\hat{X}_i\hat{X}_j] - d_i E[\hat{X}_j] - d_j E[\hat{X}_i] + d_i d_j \\ &= E[\hat{X}_i\hat{X}_j] - d_i d_j - d_j d_i + d_i d_j \\ &= E[\hat{X}_i\hat{X}_j] - d_i d_j \\ &= \mathrm{Cov}(\hat{q}, \hat{p}). \end{aligned} \tag{2.31}$$

To completely know a Gaussian state it is sufficient to determine its displacement d and its convariance matrix Σ.

This work focus on the analysis of 1-mode Gaussian states obtained from thermal states. There are two chapters of analysis. The first one presents a method of learning the variances of the quadratures from Fock population measurements of a squeezed thermal state. All the computational and statistical tools needed in both chapters are presented together with the results. The second one presents a method of analysis of blue sideband (BSB) measurements data from trapped ion systems. It includes a proposal of a model to this kind of measurement and its analysis with both simulated and real data. The model depends on the Fock population of the state measured. The statistical tools used are the same from chapter 3 and any other new knowledge needed is presented during the chapter.

3 SQUEEZED THERMAL STATE ANALYSIS

3.1 Squeezed Thermal States

Squeezed thermal states can be obtained by different processes. Thermal noise can be added to a squeezed state, squeezing can be applied to a thermal state, or both heating and squeezing can happen simultaneously. All the resulting states are Gaussian and can be described by the parameters $\bar{n}$ (the mean thermal Fock number, which quantifies the temperature) and r (the strength of the squeezing) (Olivares 2012).

Let us consider the case where squeezing is applied to a thermal state. The thermal state has the density operator $\hat{\rho}_{th}$ given by Eq. (2.24):

$$\hat{\rho} = \hat{\rho}_{th}. \tag{3.1}$$

The state is then squeezed, resulting in the new state

$$\hat{\rho}_s = \hat{S}(r)^{\dagger}\hat{\rho}\hat{S}(r). \tag{3.2}$$

Since Squeezed thermal states are examples of Gaussian states, their Wigner distributions are Gaussian functions. A single-mode squeezed thermal state has a two-dimensional Wigner function given by:

$$W_s(q,p) = \frac{1}{2\pi|\Sigma|^{-1}} \exp\left[-\frac{1}{2}X^T\Sigma^{-1}X\right], \tag{3.3}$$

since there is no displacement, which means $d = 0$. Consequently, all the thermal and squeezing information is encoded in the covariance matrix.

Fock state population measurements have no phase dependence. Therefore we cannot obtain a full estimate of Σ because all phase rotations of Σ give the same Fock distribution. To overcome this, we estimate a diagonal Σ with the quadrature variances $V_q = \langle\hat{q}^2\rangle - \langle\hat{q}\rangle^2 \leq V_p = \langle\hat{p}^2\rangle - \langle\hat{p}\rangle^2$:

$$\Sigma = \begin{pmatrix} V_q & 0 \\ 0 & V_p \end{pmatrix}. \tag{3.4}$$

In a more detailed way, non-displaced gaussian states can be described by a general covariance matrix written in the form $R(\phi)\Sigma R(\phi)^T$, where $R(\phi)$, the rotation matrix, is given by

$$R(\phi) = \begin{pmatrix} \cos\phi & \sin\phi \\ -\sin\phi & \cos\phi \end{pmatrix}. \tag{3.5}$$

So, for a diagonal covariance matrix Σ with V_q and V_p there is an infinite set phases associated to the same variances. Since we want to estimate the diagonal elements only, we can use a particular phase over all possible values. That is why we set $\phi = 0$. And this is the Gaussian state we use in all of our simulations in this chapter. For a squeezed thermal state, the variances are related to the squeezing and temperature by

$$\begin{aligned} V_q &= \frac{1}{2}(2\bar{n}+1)e^{-2r}, \\ V_p &= \frac{1}{2}(2\bar{n}+1)e^{2r}. \end{aligned} \tag{3.6}$$

The experiment provides a list with the number of occurrences of each Fock state obtained from N measurements. The probability of finding the system in a specific Fock number n is

$$P(n|V_q,V_p) = \mathrm{Tr}\{\hat{\rho}\,|n\rangle\langle n|\}, \tag{3.7}$$

where $\hat{\rho}$ is the density operator of the state. This probability could be calculated by overlapping the unknown state's Wigner function $W(q,p)$ and the n^{th} Fock state's Wigner function $W_n(q,p)$:

$$P(n|V_q,V_p) = 2\pi \iint_{-\infty}^{\infty} W(q,p)W_n(q,p)dq\,dp, \tag{3.8}$$

where $W_n(q,p)$ is

$$W_n(q,p) = \frac{(-1)^n}{\pi}e^{-q^2-p^2}L_n(2q^2,2p^2), \tag{3.9}$$

and $L_n(2q^2,2p^2)$ are the Laguerre polynomials.

A similar approach as the one described in (Dodonov *et al.* 1994) can be used to obtain $P(n|V_q,V_p)$. In this case, we calculate the diagonal elements of the density matrix in the coherent state basis, using the overlap relation

$$\langle\alpha|\,\hat{\rho}\,|\beta\rangle = \frac{1}{2\pi}\iint_{-\infty}^{\infty} W(q,p)W_{\beta\alpha}(q,p)dq\,dp, \tag{3.10}$$

where $|\alpha\rangle$ and $|\beta\rangle$ are coherent states and $W_{\beta\alpha}$ is the Wigner function of $|\beta\rangle\langle\alpha|$.

The result of the integral for squeezed thermal states is expressed, in terms of 2D Hermite polynomials $\mathbf{H}_{mn}^{\{R\}}(0,0)$, as:

$$\langle\alpha|\,\hat{\rho}\,|\beta\rangle = P(0|V_q,V_p)\exp\left[\frac{-(|\alpha|^2+|\beta|^2)}{2}\right] \times \sum_{m,n=0}^{\infty}\frac{\alpha^n\beta^{*m}}{m!\,n!}H_{mn}^{\{R\}}(0,0), \tag{3.11}$$

where R is a symmetric 2×2 matrix whose elements are

$$\begin{aligned} R_{11} = R_{22} &= \frac{2(V_p - V_q)}{1 + 2(V_q + V_p) + 4(V_q V_p)} \\ R_{12} = R_{21} &= \frac{1 - 4V_p V_q}{1 + 2(V_q + V_p) + 4(V_q V_p)}. \end{aligned} \tag{3.12}$$

We can also compute $\langle \alpha | \hat{\rho} | \beta \rangle$ by expanding each of the coherent states in the Fock basis to obtain

$$\langle \alpha | \, \hat{\rho} \, | \beta \rangle = \exp\left[\frac{-(|\alpha|^2 + |\beta|^2)}{2}\right] \sum_{m,n=0}^{\infty} \frac{\alpha^n \beta^{*m}}{(m!\, n!)^{\frac{1}{2}}} \rho_{mn}. \tag{3.13}$$

By comparing Eq. (3.11) and Eq. (3.13), (Dodonov *et al.* 1994) derives the expression for the diagonal density matrix elements $\rho_{nn} = P(n|V_q, V_p)$:

$$P(n|V_q, V_p) = P(0|V_q, V_p) \frac{\mathbf{H}_{nn}^{\{R\}}(0,0)}{n!}, \tag{3.14}$$

where

$$P(0|V_q, V_p) = \left[0.25 + V_p V_q + 0.5\,(V_p + V_q)\right]^{-1/2}, \tag{3.15}$$

$$\mathbf{H}_{nn}^{\{R\}}(0,0) = n! \left(\frac{\left[0.5 + 2V_p V_q - (V_p + V_q)\right]}{\left[0.5 + 2V_p V_q + (V_p + V_q)\right]} \right)^{n/2} Q_n(f), \tag{3.16}$$

$Q_n(f)$ is the Legendre polynomial of order n, and

$$f = \frac{-(1 - 4V_q V_p)}{\left[(4V_q V_p + 1)^2 - 4(V_q + Vp)^2\right]^{1/2}}. \tag{3.17}$$

The function $P(n|V_q, V_p)$ obtained using Eq. (3.14) was faster to calculate than using Eq. (3.8), though the two expressions give the same results. Therefore, we use the probability distribution obtained by Eq. (3.14) in our code. The probability function for squeezed thermal states can also be obtained as in (Marian 1992; Marian and Marian 1993).

3.2 Fitting Method

The problem of estimating parameters from data can be stated as to capture the main information of a system by fitting a model to a given dataset. However experimental data comes with errors, that we represent here by ε. So, given a set of N_p data points (t_i, u_i) with $i = 1, ..., N_p$ and a model function

$$M = M(t|\mathbf{y}), \tag{3.18}$$

where $\mathbf{y}$ is a vector of parameters to be estimated, we can write $u_i = M(t_i|\mathbf{y}) + \varepsilon_i$. One may chose to get data such that $N_p = \dim(\mathbf{y})$ and solve a system of equations. However u_i comes with noise and this method does not consider all the data measured. A more appropriate procedure used to determine the vector of unknown parameters is to minimize the sum of squared residuals, given by

$$\min \sum_{i=1}^{m} r_i^2(\mathbf{y}) = \min \sum_{i=1}^{m} \left[u_i - M(t_i|\mathbf{y})\right]^2 . \tag{3.19}$$

This is known as the Least-Squares method (Hansen P. C. and Scherer 2013).

A common assumption when using this method is that all measurements u_i have the same distribution of ε_i and, consequently, the same standard deviation $\sigma_i = \sigma$. Therefore, all u_i have the same importance in the sum of r_i^2. It means that Eq. (3.19) can be written as a weighted sum

$$\min \sum_{i=1}^{m} w_i \left[r_i(\mathbf{y})\right]^2 , \tag{3.20}$$

with all weights $w_i = 1$. However, it may happen that different measurements u_i have different uncertainties associated. When this happens, setting $w_i = 1$ means to give the same importance in the estimation process to measurements with big and small uncertainties. When ε_i is normally distributed we can write

$$\varepsilon_i \propto \exp\left\{ -\frac{1}{2} \frac{\left[u_i - M(t_i|\mathbf{Y})\right]}{\sigma_i} \right\}^2 . \tag{3.21}$$

Comparing this to Eq. (3.20), we can write the weights as $w_i = 1/\sigma_i^2$, the inverse of the squared standard deviation of the measurement u_i. These weights can be obtained from a sets of measurements from which the standard deviation can be calculated directly. However that amount of data may not be available, requiring one to estimate those errors from a single dataset. When dealing with data obtained from Fock states measurements or blue sideband measurements it is possible to model the detection probability by considering those kind of measurements as Bernoulli trials, with only two possible results, detecting or not, and that when repeated N times result in a Binomial distribution of probabilities of detecting an specific Fock number $|n\rangle$ or a "bright" for an specific pulse duration t.

Let us consider a dataset of measurements of a set of Fock numbers or "brights" observed for different blue sideband (BSB) pulse durations, and represent it by $\{f\}$. In trapped ion systems there is no phase sensitive nor direct Fock population measurements available. A common way used to measure the ion's state is to couple its electronic state to the motional

state by applying a blue sideband laser (BSB) pulse during a fixed time, and measuring its state-dependent fluorescence. The probability of detecting fluorescences ("brights") depends on both the spin and ion's motional Fock population. It also depends on how long the pulse is applied to the ion. Thus, the data provided by the experiment is a set of relative frequencies of fluorescence detection for different pulse duration times. More details about the model will be presented in next chapter.

The experiments measures the number k_i of times the detection occurs over a total of N measurements (repetitions for ion experiments) such that $f_i = k_i/N$ for $i = 1, ..., i_{max}$ is the relative frequency detected, where i_{max} may be the maximum Fock number or the maximum number of pulse duration considered. The weights $w_i = 1/\sigma^2(f_i)$ quantify the uncertainty in the measurement f_i. A binomial distribution has success probability $P_i = P_i(k_i|\mathrm{p}_i)$, where p_i is the probability of the measurement to occur and $f_i \to \mathrm{p}_i$ as $N \to \infty$. For this distribution, $\sigma^2(k_n) = N\mathrm{p}_n(1-\mathrm{p}_n)$, but we need to estimate $\sigma^2(f_i)$, that can be done by using the Maximum Likelihood Estimator (MLE). The MLE for the binomial success probability p_i is $\hat{\mathrm{p}}_i = k_i/N$, allowing us to estimate $\sigma^2(f_i) \approx \sigma^2(\hat{\mathrm{p}}_i)$. We can estimate $\sigma^2(\mathrm{p}_i)$ by considering the definition of the variance of a random variable X: the expected value of the squared difference between X and its expected value,

$$\sigma^2(X) = E\left[(X - E[X])^2\right]. \tag{3.22}$$

Consequently,

$$\sigma^2(bX) = E\left[(bX - E[bX])^2\right] = b^2\sigma^2(X), \tag{3.23}$$

where b is a scalar. So the variance of $\hat{\mathrm{p}}_i = \frac{1}{N}k_i$ can be written as

$$\sigma^2(\hat{\mathrm{p}}_i) = \frac{\sigma^2(k_i)}{N^2}. \tag{3.24}$$

We can finally find the variance of f_i as

$$\sigma^2(f_i) \approx \frac{N\hat{\mathrm{p}}_i(1-\hat{p}_i)}{N^2} \tag{3.25}$$

$$= \frac{k_i(N-k_i)}{N^3}. \tag{3.26}$$

It is important to note that $w_i = 1/\sigma^2(f_i)$ depends on $1/k_i$, and that may be a problem when $k_i = 0$, which will happen frequently with highly pure squeezed states. The weighted sum of squared residuals is given by:

$$\Delta(V_q, V_p) = \sum_{n=0}^{n_F} w_n \left[P(n|V_q, V_p) - f_n\right]^2, \tag{3.27}$$

where w_n is the weight associated with the n^{th} measurement. Our estimates will be those values of V_q and V_p that minimize $\Delta(V_q, V_p)$. However, not all pairs of variances are allowed because the Heisenberg restriction imposes $V_q \times V_p \geq 0.25$. We also impose the constraints $V_q \leq V_p$, $V_q > 0$, and $V_p > 0$.

To overcome this problem, we use Bayesian inference (Aitkin 2010) to estimate $\sigma^2(f_n)$. In classical statistics it is possible to estimate a given parameter Θ associated to a system by doing a set of measurements of it, where that parameter is considered to be fixed. In the Bayesian statistics, Θ has a probability function associated (a prior distribution) based on any previous information about the system. Then, after a set of measurements, the prior function is updated to a posterior distribution. Mathematically, the starting point is the Bayes's rule

$$P(\Theta|U) = P(U|\Theta)P(\Theta)/P(U), \tag{3.28}$$

where U is the data, $P(\Theta|U)$ is the posterior function, $P(\Theta)$ is the prior function, $P(U|\Theta)$ is the likelihood function, and $P(U)$ is the marginal distribution given by $P(U) = \int P(U|\Theta)P(\Theta)d\Theta$. The Bayes rule can be rewritten as

$$P(\mathrm{p}_n|k_n) = P(k_n|\mathrm{p}_n)P(\mathrm{p}_n)/P(k_n), \tag{3.29}$$

where now $P(\mathrm{p}_n)$ is the prior probability distribution associated to the measurement of $|n\rangle$.

A direct choice for the likelihood $P(k_n|\mathrm{p}_n)$, considering this specific kind of measurement, is the binomial distribution,

$$P(k_n|\mathrm{p}_n) = \binom{N}{k_n} {\mathrm{p}_n}^{k_n} (1-\mathrm{p}_n)^{N-k_n}.$$

Since the likelihood function is binomial, an appropriate choice for the prior $P(\mathrm{p}_n)$ is a beta distribution given by

$$P(\mathrm{p}_n) = \frac{{\mathrm{p}_n}^{\nu-1}(1-\mathrm{p}_n)^{\eta-1}}{\mathrm{Beta}(\nu,\eta)}, \tag{3.30}$$

where ν and η are the shape parameters and $\mathrm{Beta}(\nu,\eta)$ is the Beta function,

$$\mathrm{Beta}(\nu,\eta) = \int_0^1 t^{\nu-1}(1-t)^{\eta-1}dt.$$

As a consequence, the posterior distribution will be also a beta distribution. Both $P(\mathrm{p}_n|k_n)$ and $P(\mathrm{p}_n)$ are called conjugate distributions and $P(\mathrm{p}_n)$ is a conjugate prior to the likelihood $P(k_n|\mathrm{p}_n)$.

The function $P(k_n)$ is given by

$$\begin{aligned} P(k_n) &= \int_0^1 P(k_n|\mathrm{p}_n)P(\mathrm{p}_n)\,d\mathrm{p}_n \\ &= \binom{N}{k_n}\frac{\int_0^1 \mathrm{p}_n{}^{k_n+\nu-1}\,(1-\mathrm{p}_n)^{N-k_n+\eta-1}\,d\mathrm{p}_n}{\mathrm{Beta}(\nu,\eta)} \\ &= \binom{N}{k_n}\frac{\mathrm{Beta}(k_n+\nu,N+\eta-k_n)}{\mathrm{Beta}(\nu,\eta)}. \end{aligned} \tag{3.31}$$

The posterior distribution is then given by

$$P(\mathrm{p}_n|k_n) = \frac{\mathrm{p}_n{}^{k_n+\nu-1}\,(1-\mathrm{p}_n)^{N-k_n+\eta-1}}{\mathrm{Beta}(k_n+\nu,N+\eta-k_n)}, \tag{3.32}$$

which is a Beta distribution with new shape parameters $\nu' = k_n+\nu$ and $\eta' = N+\eta-k_n$ and variance

$$\sigma^2(\mathrm{p}_n|k_n) = \frac{(k_n+\nu)(N+\eta-k_n)}{(\nu+N+\eta)^2(\nu+N+\eta+1)}. \tag{3.33}$$

We use this variance when computing the weights $w_n = 1/\sigma^2(\mathrm{p}_n|k_n)$ in the weighted sum of squared residuals, which ensures that the weights are finite when $k_n = 0$.

Figure 4 presents the behavior of weights calculated with priors having different values of N and different shape values. The graphs show that for $N \geq 100$, which is easily achievable in experiments, the weights are not very sensitive to the choices for η and ν. Odd Fock numbers have higher weights because we are testing a nearly pure squeezed state, which has low probability for containing odd Fock numbers.

3.3 Testing

3.3.1 Simulated Experiments

To test our estimator we feed it with simulated data from a known state and compare it with the output. It allows us to do tests for different sets of parameters, covering different possible states such as thermal states with different temperatures, squeezed thermal states with different temperatures and compression factors, squeezed states and any other 1-mode Gaussian state, providing a way to obtain as much data as needed for the statistical analysis. The simulated experiment must consider a probability of measurement p_n and a number of measurements k_n

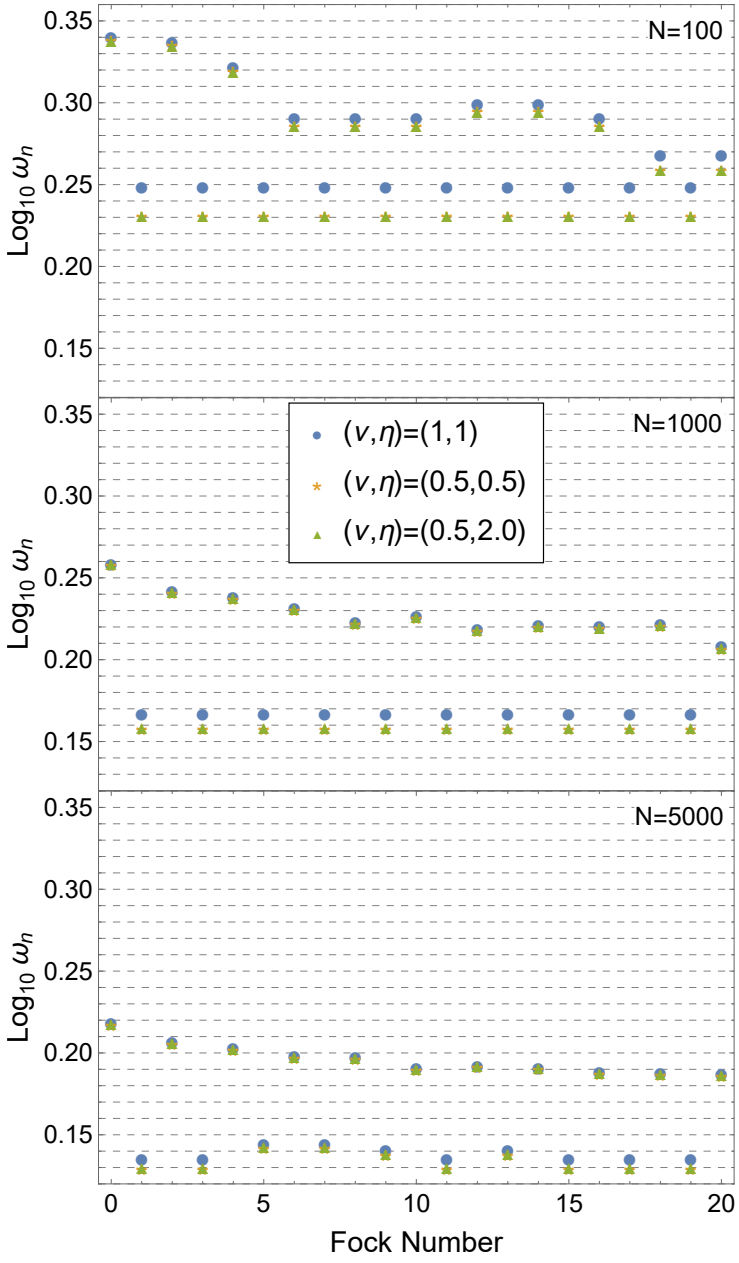

Figure 4 – Graphs showing $\log_{10} w_n$ of the weights used in the least-squares fit versus n for measurements of the quantum state with squeezing $r = 2.5$ and thermal average Fock number $\bar{n} = 0.01$, for three different numbers N of measurements and for different values of the prior distribution's shape parameters ν and η. We see that the weights are not very sensitive to the prior distribution's shape parameters ν and η, and the closeness increases for increasing N. We observed similar behavior for other choices of r and $\bar{n}$.

for each Fock number that satisfy the relations

$$\begin{aligned} \sum_{n=0}^{n_{max}} p_n &= 1, \\ \sum_{n=0}^{n_{max}} k_n &= N, \end{aligned} \tag{3.34}$$

where n_{max} is the maximum Fock number considered. The best distribution that describes the probability of measuring a population of Fock states given by $K = \{k_i\}$, over a total number of measurements N, is given by the multinomial distribution

$$f(K) = \frac{N!}{k_1!k_2!\ldots k_n!}\, p_1^{k_1}\, p_2^{k_2} \ldots p_n^{k_n}. \tag{3.35}$$

Its marginal distributions must describe the probability of measuring k_n over a total of N with a probability p_n, as we can see by doing

$$\begin{aligned} f_n(k_n) &= \sum_{k_1\, k_2 \ldots k_{n-1}} \frac{N!}{k_1!k_2!\ldots k_n!}\, p_1^{k_1}\, p_2^{k_2} \ldots p_n^{k_n} \\ &= \sum_{k_1\, k_2 \ldots k_{n-1}} \frac{N!}{k_1!k_2!\ldots k_n!}\, p_1^{k_1}\, p_2^{k_2} \ldots p_n^{k_n}\, \frac{(N-k_n)!(1-p_n)^{N-k_n}}{(N-k_n)!(1-p_n)^{N-k_n}}. \end{aligned} \tag{3.36}$$

The elements associated to k_n can be placed outside of the summation resulting in the binomial distribution times a sum:

$$f_n(k_n) = \frac{N!\, p_n^{k_n}\, (1-p_n)^{N-k_n}}{k_n!\,(N-k_n)!} \sum_{k_1\, k_2 \ldots k_{n-1}} \frac{(N-k_n)!}{k_1!k_2!\ldots k_{n-1}!}\, \frac{p_1^{k_1}\, p_2^{k_2} \ldots p_{n-1}^{k_{n-1}}}{(1-p_n)^{N-k_{n-1}}} \tag{3.37}$$

Rewriting $N-k_n = k_1+k_2+\ldots+k_{n-1}+k_n-k_n = \sum_{i=1}^{n-1} k_i$ and replacing in the previous equation we obtain

$$f_n(k_n) = \frac{N!\, p_n^{k_n}\, (1-p_n)^{N-k_n}}{k_n!\,(N-k_n)!} \sum_{k_1\, k_2 \ldots k_{n-1}} \frac{(N-k_n)!}{k_1!k_2!\ldots k_{n-1}!}\, \frac{\prod_{i=1}^{n-1} p_i^{k_i}}{\prod_{i=1}^{n-1}(1-p_n)^{k_i}}. \tag{3.38}$$

If we do the substitutions $p_i' = \frac{p_i}{1-p_n}$ and $N' = N-k_n$, the function in the sum becomes a multinomial distribution with probabilities p_i', where

$$\sum_{i}^{n-1} p_i' = \frac{p_1+p_2+\ldots+p_{n-1}}{1-p_n} = \frac{1-p_n}{1-p_n} = 1. \tag{3.39}$$

With this sum equal to 1, we obtain the following expression for the marginal distribution:

$$f_n(k_n) = \frac{N!\, p_n^{k_n}\, (1-p_n)^{N-k_n}}{k_n!\,(N-k_n)!}. \tag{3.40}$$

And, as expected, this is a binomial. So for each Fock number there is a binomial distribution that describes the probability of obtaining k_n measurements over a total of N with an associated

probability p_n. Once the simulated datesets are available, the next step is to analyse all the data. This analysis consists in obtaining the point estimates from the simulated data from a specific state and calculating its uncertainty.

A common way to compare the performance of two estimators is calculating the mean squared error of the estimates obtained from fitting an specific dataset. It can be calculated as the expected value

$$\mathrm{MSE}(\hat{\theta}) = E[(\hat{\theta} - \theta)^2], \tag{3.41}$$

where $\hat{\theta}$ is the estimator and θ the true value. Expanding the expectation above, we obtain

$$\begin{aligned} \mathrm{MSE}(\hat{\theta}) &= E[\hat{\theta}^2 + \theta^2 - \hat{\theta}\theta - \theta\hat{\theta}] \\ &= E[\hat{\theta}^2] + E[\theta^2] - E[\hat{\theta}\theta] - E[\theta\hat{\theta}] \\ &= E[\hat{\theta}^2] + \theta^2 - 2\theta E[\hat{\theta}] \\ &= E[\hat{\theta}^2] + (E[\hat{\theta}] - \theta)^2 - E[\hat{\theta}]^2 \\ &= \sigma^2[\hat{\theta}] + \mathrm{Bias}[\hat{\theta}, \theta]^2. \end{aligned} \tag{3.42}$$

The estimator's performance is connected to its variance and bias. When there is no bias the estimator is called unbiased and its mean squared error is equal to its variance. Small standard deviation together with big bias may result in a small probability of the estimator to obtain estimates that are close to the true value, since the distribution of point estimates will be distributed around a value that is far from θ. As a result the trade-off between bias and standard deviation needs to be included in our analysis.

The data analysis also includes estimates of bias, confidence intervals, and their coverage probabilities together with the relation between standard deviation and bias and its tradeoff. For various choices for $\bar{n}$ and r we simulated 100 experiments. For each experiment, the Fock distribution is measured N times and an estimate of $\bar{n}$ and r is produced. From those experiments, we calculated the mean fidelity and report its dependence on N for $\bar{n} = (0.001, 0.01, 0.1, 2)$ and $r = (0, 1.0, 2.5)$. (Burd *et al.* 2019) reported squeezing of $r = 2.26 \pm 0.02$.)

Of course, only a finite number of Fock states can be resolved in an experiment. (Burd *et al.* 2019) reported the resolution of 20 Fock states for ion motion, and (Lolli *et al.* 2012) and (Morais *et al.* 2020) resolve 29 and 16 photonic Fock states, respectively, with transition edge sensors. In our simulations, we assume that the detectors can resolve Fock numbers 0 through 20, but they cannot distinguish higher Fock numbers. Thus we have 22 possible

measurement results, with the first 21 being Fock numbers 0 through 20 and the last containing all events with Fock numbers ≥ 21. This provides enough information for our tests, which have $r \leq 2.5$ and $\bar{n} \leq 2$. During the simulated experiment the probability of getting a set of counts for $n = 0$ to 21 over a total of N measurements can be calculated by a multinomial distribution for $P(n|V_q, V_p)$ and N total measurements. We used Mathematica to generate samples from a multinomial distribution. Thus we simulate all the data needed to evaluate our method.

Quantum state fidelity, F, measures the closeness of two states ρ_1 and ρ_2:

$$F(\rho_1, \rho_2) = \left[\mathrm{Tr}\left(\sqrt{\sqrt{\rho_1}\rho_2\sqrt{\rho_1}} \right) \right]^2 . \tag{3.43}$$

We use the quantum state fidelity between the true state and our estimate to quantify the accuracy of our estimator. Because we are estimating squeezed thermal states, we rewrite the fidelity as (Marian and Marian 2012):

$$F(\rho_1, \rho_2) = (\sqrt{\Xi + \Lambda} + \sqrt{\lambda})^{-1}, \tag{3.44}$$

where Ξ and Λ are given by

$$\begin{aligned} \Xi &= \det(\Sigma_1 + \Sigma_2), \\ \Lambda &= 4 \det\left(\Sigma_1 + \frac{i}{2} J \right) \det\left(\Sigma_2 + \frac{i}{2} J \right). \end{aligned} \tag{3.45}$$

Σ_1 and Σ_2 are the single mode covariance matrices for each mode, and J is

$$J = \begin{pmatrix} 0 & 1 \\ -1 & 0 \end{pmatrix} . \tag{3.46}$$

Figure 5 plots the mean infidelity, $1 - \langle \text{Fidelity} \rangle$, averaged over 100 simulated experiments using different shape parameters η and ν (used to specify the prior distribution when calculating the posterior used to estimate the weights) on the fidelities as a function of N for three different states. For any N and the three states chosen, $\eta = \nu = 1$ (corresponding to the uniform prior distribution) performs better than the other tested pairs of shape parameters. For all following simulations we use $\eta = \nu = 1$. Fig. 5 also shows the importance of using weights, specially for high squeezing states ($r = 2.5$).

Figure 6 presents $1 - \langle \text{Fidelity} \rangle$ versus N for three different squeezing values and four values of $\bar{n}$. States with higher squeezing require larger N to obtain high fidelity estimates, but the fidelities are less sensitive to $\bar{n}$. For a state with $r = 2.5$, $\bar{n} = 0.1$, after 10100 measurements, from 100 simulated experiments, we obtain an average fidelity of 0.9991, and the standard deviation of the fidelity estimates is 0.0011.

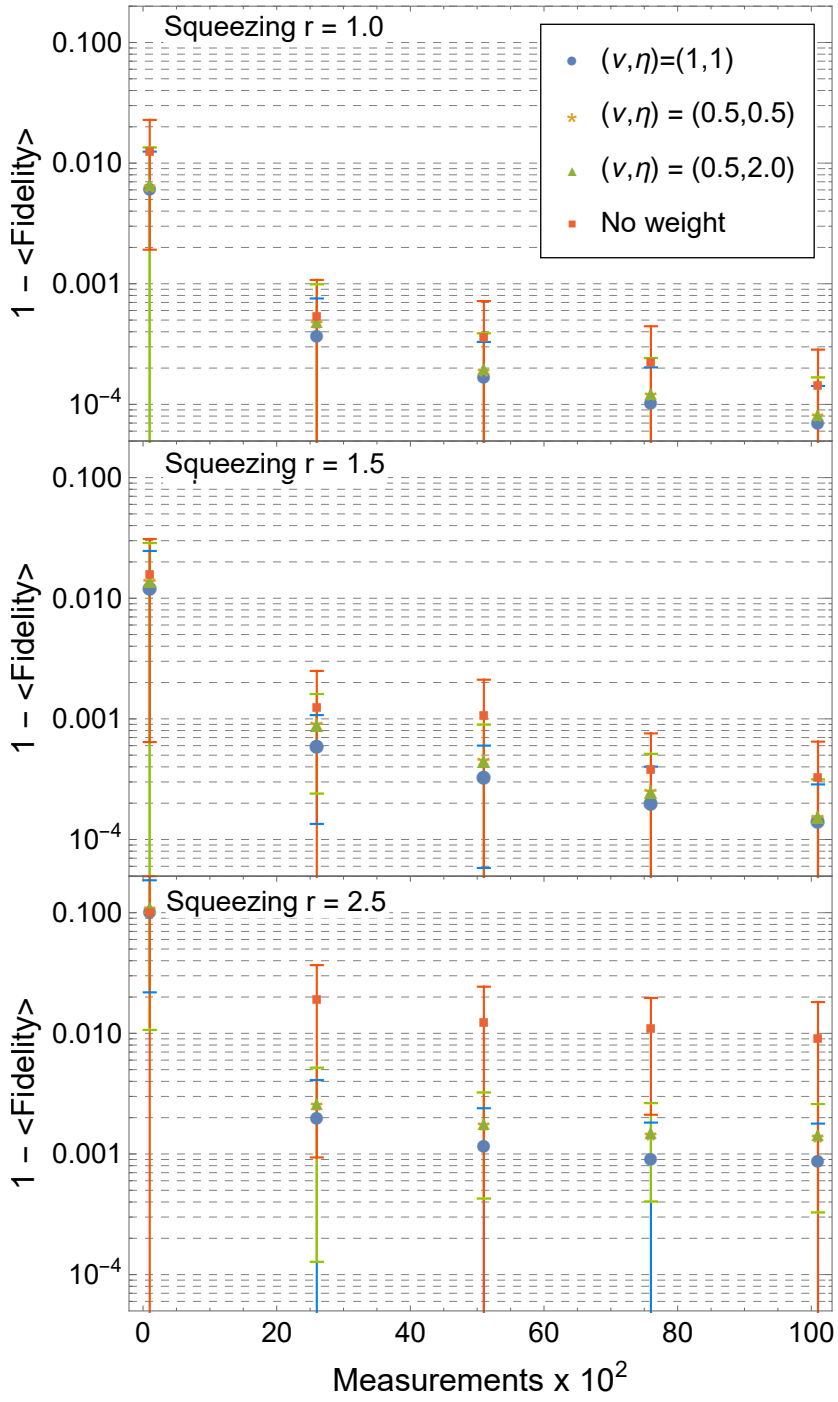

Figure 5 – $1 - \langle \text{Fidelity} \rangle$, the mean infidelity averaged over 100 simulated experiments, and the standard deviation of the 100 infidelities as a function of the number N of measurements for $\bar{n} = 0.01$, three values of squeezing, and different choices the shape parameters ν and η that determine the weights used in the weighted least squares estimator.

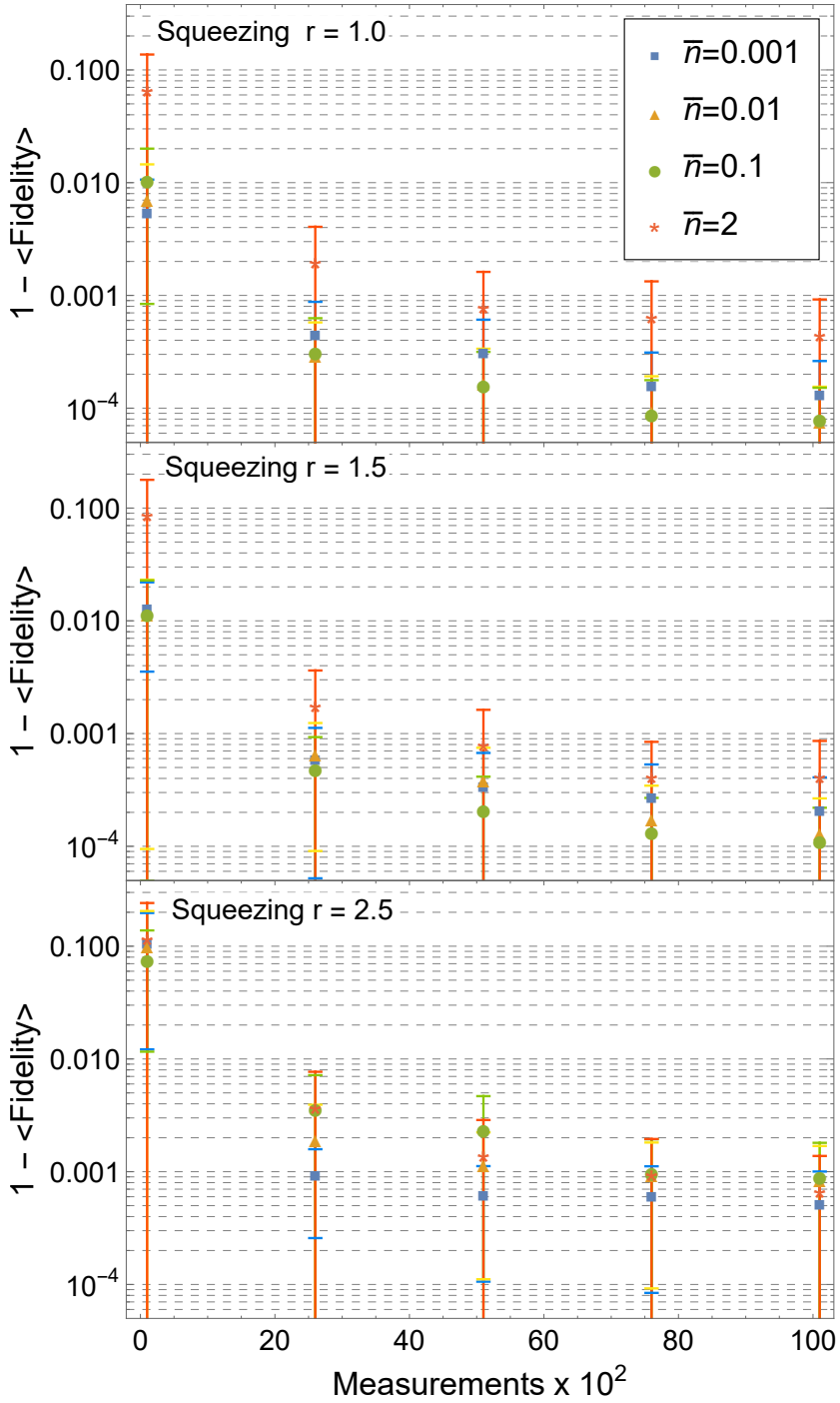

Figure 6 – 1 – ⟨Fidelity⟩ and the standard deviation of the fidelity estimates as a function of the number of measurements for different $\bar{n}$'s.

3.3.2 Confidence Intervals

We characterize uncertainty in our estimates using confidence intervals. We do it by estimating a set of values from the data, provided that it may contain the true value. So, given the data $\mathbf{f}$ there exist a pair of functions such that $C_i(\mathbf{f}) \leq C_j(\mathbf{f})$ and the inference

$$C_i(\mathbf{f}) \leq \Theta \leq C_j(\mathbf{f}) \tag{3.47}$$

can be made. The interval $[C_i(\mathbf{X}), C_j(\mathbf{X})]$ is the interval estimate associated to the data. Although an interval estimate provides a set of values instead of a point estimate, it adds to the analysis some guarantee of covering the parameter of interest. This guarantee is represented by the coverage probability, that means the chance of the estimated intervals covering Θ. These intervals are also known as confidence intervals with a confidence level, that impacts directly on its size. A larger confidence level may result in larger interval, and a smaller confidence level in a smaller interval.

A confidence interval (CI) of confidence level $(1-2\beta)$ (with $0 \leq \beta \leq 1$) for an estimated parameter has the property that with probability $(1-2\beta)$ when the experiment is performed and the CI calculated, the CI will contain the true value of the parameter. Bootstrap methods (Efron and Tibshirani 1993) provide a way to calculate CIs, based on two steps: using simulations to build a set of estimates and applying an algorithm to the simulated estimates to produce the interval. For the first step, we use a "parametric bootstrap" in which estimates of V_q and V_p obtained from the original experiment are used to simulate experiments N_B times according to the model described by Eq. (3.14), producing N_B pairs of simulated estimates of V_q and V_p (or equivalently r and $\bar{n}$).

The Percentile Method (Efron and Tibshirani 1993; Carpenter and Bithell 2000) was the first used to calculate our confidence. For an estimator $\hat{\Theta}$ of some parameter Θ and an ordered set of simulated bootstrap estimates $B_R = (\hat{\Theta}_1, \hat{\Theta}_2, ..., \hat{\Theta}_{N_B})$, the $(1-2\beta)$ CI is $[\hat{\Theta}_l, \hat{\Theta}_m]$, where

$$\begin{aligned} l &= \lfloor N_B \beta \rfloor \\ m &= \lfloor N_B (1-\beta) \rfloor. \end{aligned} \tag{3.48}$$

We performed a test of the Percentile Method on three different reference states given by fixed $\bar{n} = 0.01$ and squeezing $r = (0, 1.0, 2.5)$. For each state, we ran 100 simulated experiments with $N = 10^4$. For each we calculated a 90% confidence interval ($\beta = 0.05$) and then estimated the coverage probabilities by the fraction of times that the confidence intervals contained the

State (r, $\bar{n}$)	V_p(1k)	V_q(1k)	r(1k)	$\bar{n}$(1k)	V_p(2k)	V_q(2k)	r(2k)	$\bar{n}$(2k)
(0, 0.01)	83%	88%	98%	94%	84%	89%	98%	93%
(1.0, 0.01)	82%	88%	87%	56%	83%	88%	86%	57%
(2.5, 0.01)	86%	58%	70%	15%	87%	59%	73%	18%

Table 1 – Table of the coverage probabilities for nominal 90% confidence intervals using the percentile method. The coverage probabilities were estimated from 100 simulated experiments using $N_B = 1{,}000$ (left) and $N_B = 2{,}000$ (right) bootstrap replicates. The coverage probabilities significantly different from 90% motivate our use of bias correction, shown in Table 3.

True r	B/σ in r	True V_p	B/σ in V_p	True V_q	B/σ in V_q	B/σ in $\bar{n}$
0	0.69	0.51	0.68	0.51	-0.68	0.069
0.5	-0.16	1.39	-0.19	0.19	0.013	-0.25
1	-0.24	3.77	-0.32	0.069	0.16	-0.64
1.5	-0.020	10.24	-0.12	0.025	-0.085	-0.90
2	0.27	27.85	0.094	0.0093	-0.44	-1.098
2.5	0.45	75.69	0.15	0.0034	-0.72	-1.40

Table 2 – Estimates of bias B divided by standard deviation σ for estimates of parameters of states with various squeezing parameters r and $\bar{n} = 0.01$. Each estimate was generated from 1,000 simulated experiments, containing $N = 10{,}000$ Fock measurements each, so some statistical fluctuation is expected. Estimates for which $|\mathrm{B}/\sigma| > 1$ indicate that the bias in the estimate is significant when compared to the statistical uncertainty in the estimate, and so bias correction may be useful.

true value, with V_q, V_p, r, and $\bar{n}$ considered independently. For comparison we tested both $N_B = 1{,}000$ and $2{,}000$. Table 1 presents the results of the test. $N_B = 1{,}000$ gives good results for lower squeezing, but as squeezing increases the coverage probabilities decrease for all parameters but V_p. Doubling the number of bootstrap simulations does not significantly improve the coverage probabilities. For $r = 2.5$, the coverage probability for $\bar{n}$ is far from expected. Coverage probabilities of around 98% are obtained for estimates of r when $r = 0$ because this is on the boundary of parameter space and no bootstrap simulation can give estimates below 0.

To understand the low coverage probabilities we explore the ratio B/σ of bias (here denoted by B) to standard deviation for estimates of parameters of different states, as shown in Table 2. Bias is the difference between the expectation value of an estimate of a parameter and the true value of that parameter. We calculated B/σ for both quadrature variances, r, and $\bar{n}$ for several states. We have previously seen that the highest squeezing considered, $r = 2.5$, presented the worst results of average fidelity, and we can see in Table 2 that high squeezing also causes large B/σ ratios. Such large B/σ ratios, especially for estimates of $\bar{n}$ at high squeezing, could be the cause of the low coverage probabilities obtained when using the percentile method to construct confidence intervals.

State $(r, \bar{n})$	V_p(1k)	V_q(1k)	r(1k)	$\bar{n}$(1k)	V_p(2k)	V_q(2k)	r(2k)	$\bar{n}$(2k)
(0, 0.01)	89%	88%	97%	97%	86%	90%	98%	97%
(1.0, 0.01)	87%	89%	88%	82%	89%	89%	89%	85%
(2.5, 0.01)	92%	89%	89%	74%	90%	86%	88%	77%

Table 3 – Table of the coverage probabilities for nominal 90% confidence intervals with bias correction, computed for the same states and data as shown in Table 1. We see the coverage probabilities significantly closer to 90%, compared to the uncorrected intervals of Table 1.

To reduce the influence of bias we use the "BC" algorithm from (Efron 1982) to calculate the CIs. The results are shown in Table 3 and were obtained using the same data used for Table 1. The bias correction provides confidence intervals with coverage probabilities closer to the specified confidence level of 90%, though the coverage probability for $\bar{n}$ is still low.

Fig. 7 shows a set of 30 example 90% intervals for $\bar{n}$ calculated for the tests presented on Tables 1 and 3. After bias correction, far more of the confidence intervals contain the true value of $\bar{n}$. For example, for the state with $r = 2.5$ and $\bar{n} = 0.01$, measured $N = 1,000$ times, when nominal 90% confidence intervals are calculated, the coverage probability for $\bar{n}$ has increased from 15% to 74% by using the bias correction. Because of the $\bar{n} \geq 0$ boundary, we expect that it will be difficult to achieve exact coverage probability for states with $\bar{n}$ near 0 using standard methods, but given the bootstrap estimates, the bias correction is easy to apply and significantly improves the coverage probability.

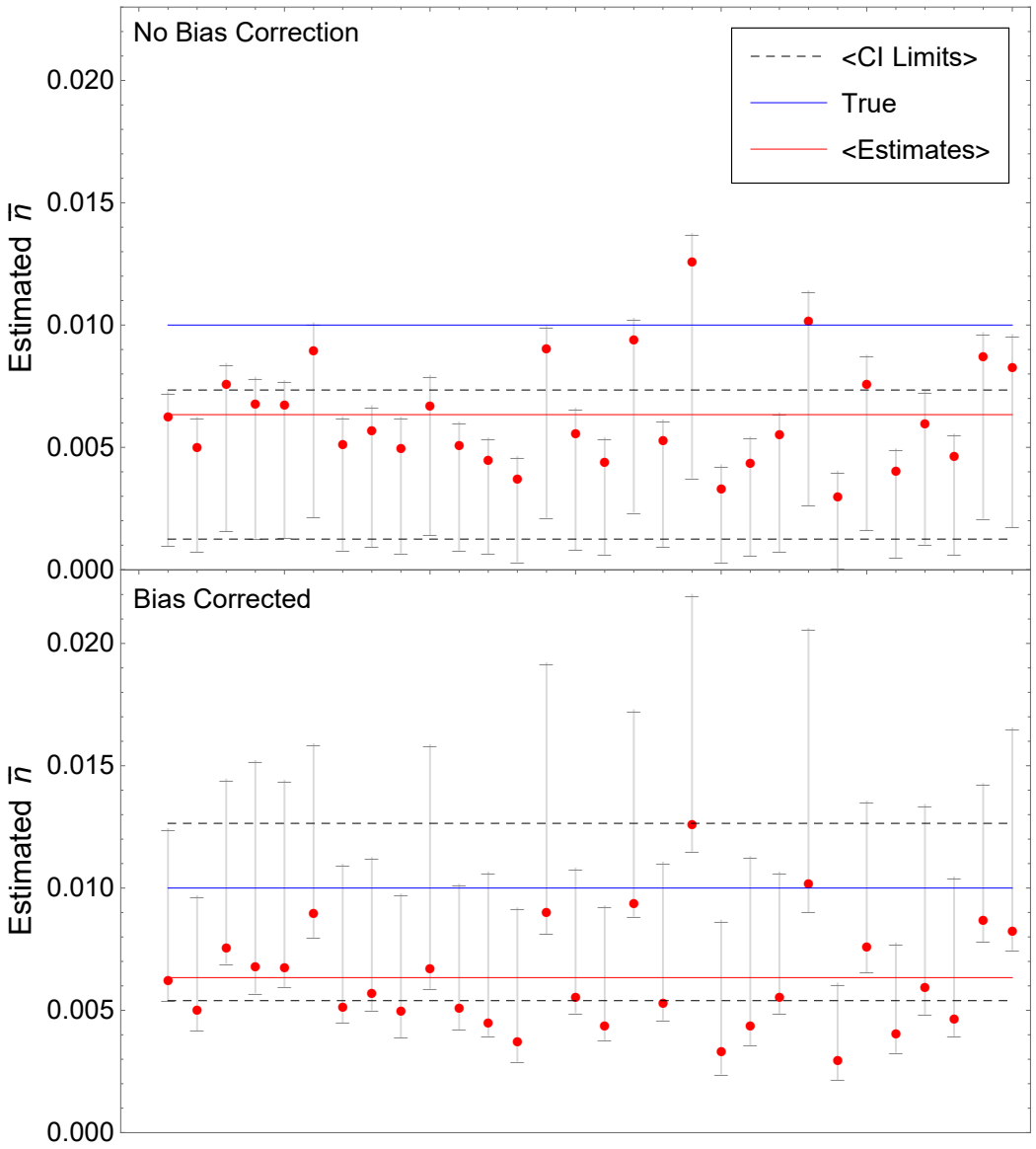

Figure 7 – Example confidence intervals for $\bar{n}$, computed with the percentile method (upper panel) and the bias correcting BC method (lower panel) arranged in arbitrary order along the horizontal axis. The true parameters are $r = 2.5$ and $\bar{n} = 0.01$. The red dots show the point estimates for $\bar{n}$, the gray error bars show the confidence intervals with and without bias correction, the blue lines show the true value of $\bar{n}$, the red lines show the mean of the point estimates, and the dashed lines show the means of the upper and lower ends of the confidence intervals.

4 SQUEEZED DISPLACED THERMAL STATES ANALYSIS

This chapter focus on the analysis of a method to learn from squeezed displaced thermal states (SDTS) data. Essentially, the whole analysis e based on blue sideband measurements obtained from a single trapped ion experiment and its steps as presented in (Burd *et al.* 2019) and more recently at (Burd *et al.* 2023). The experiment aims to produce displaced thermal states. These states are then squeezed and then anti-squeezed to generate, ideally, a new displaced thermal state with modified displacement. However, it may happen that the reverse squeezing protocol does not work perfectly resulting in residual squeezing in the final state. Therefore both the state obtained after squeezing the displaced thermal state and the one obtained after reversing the squeezing are SDTS. Displaced thermal states (DTS) are included in the analysis in order to compare displacements before and after squeezing + reverse-squeezing. Moreover, the amount of squeezing and residual squeezing can be better analysed from squeezed thermal states (STS) both after squeezing and after squeezing and anti-squeezing. Finally, the thermal state at which the ion is started must be included. The final state is a SDTS represented by the density operator

$$\hat{\rho}_{SDTS} = \hat{S}(\zeta)\hat{D}(\alpha)\,\hat{\rho}_{th}\hat{D}^{\dagger}(\alpha)\hat{S}^{\dagger}(\zeta) \tag{4.1}$$

Thus, the parameters to be estimated are $|\alpha|$, r, $\bar{n}$, θ and ϕ, that are the amount of displacement, squeezing, temperature, displacement phase and squeezing phase, respectively. Here, both phases are related such that the phase to be considered is the relative phase $\varphi = \theta - \frac{\phi}{2}$.

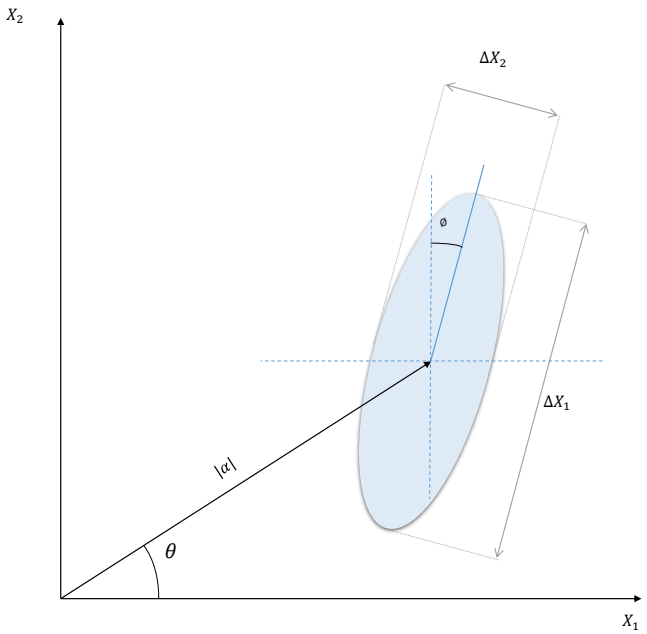

Figure 8 – Uncertainty region of a squeezed displaced thermal state.

Fig. 8 presents a plot of the region of standard deviation associated to the quadratures, here written as the components $X_1 = q$ and $X_2 = p$.

The data considered is a set of measurements obtained for different blue sideband laser pulse duration since that duration interfere in the interaction of the pulse with the spin of the ion. For a pulse duration t_i, each measurement consist in detecting or not fluorescence from the ion. After repeating the process N times the number of "brights" detected are k_i. The relative frequency of detection is given by $f_i = K_i/N$ and it is related to the probability of detecting the spin down state by $f_i \approx P_{\downarrow}(t_i)$. That probability is given by (Burd *et al.* 2019)

$$P_{\downarrow}(t) = \frac{1}{2} + \frac{1}{2}\sum_{n=0}^{\infty} P(n) e^{-\gamma_n t}\cos\Omega_n t, \tag{4.2}$$

where Ω_n is the Rabi frequency and γ_n is a decay rate constant. Both depends on the Fock number n of the ion's motional state and are considered to be given by (Burd *et al.* 2019)

$$\begin{aligned} \Omega_n &= \Omega\sqrt{n+1}, \\ \gamma_n &= \gamma\sqrt{n+1}. \end{aligned} \tag{4.3}$$

For a SDTS, the Fock population $P(n)$ is in the form $P(n||\alpha|, r, \bar{n}, \varphi)$ and it can be obtained from the representation of $\hat{\rho}_{SDTS} = \hat{\rho}_{final} = \hat{\rho}_f$ in the coherent states basis by doing

$$\begin{aligned} \langle\beta_1|\hat{\rho}_f|\beta_2\rangle &= \sum_{l=0}^{\infty}\sum_{m=0}^{\infty} e^{-|\beta_1|^2/2} e^{-|\beta_2|^2/2} \frac{\beta_1^{*l}\beta_2^m}{\sqrt{l!m!}} \langle m|\hat{\rho}_f|n\rangle \\ &= \sum_{l,m=0}^{\infty} e^{-(|\beta_1|^2+|\beta_2|^2)/2} \rho_{f\,lm} \frac{\beta_1^{*l}\beta_2^m}{\sqrt{m!n!}}, \end{aligned} \tag{4.4}$$

where now $\rho_{f\,lm}$ are the elements of the density operator in the Fock basis and $\langle\beta_1|\hat{\rho}_f|\beta_2\rangle$ is the overlap between the Gaussian Wigner function for SDTS and the Wigner function of the operator $|\beta_1\rangle\langle\beta_2|$. The right side of the previous equation can be written in terms of Hermite polynomials by using its generating function $e^{2xz-z^2} = \sum_{n=0}^{\infty} H_n(x) z^n/n!$. When compared with the result of the left side, as done by (Marian 1992), the expression for the diagonal elements of the density matrix $\rho_{f\,nn} = P(n)$ are given by

$$P(n) = \pi Q(0)(-1)^n 2^{-2n}(A+|B|)^n \sum_{k=0}^{\infty} f_k(A,B) H_{2k}\left(i\frac{\mathrm{Im}(C)}{(A-|B|)^{1/2}}\right) H_{2(l-k)}\left(i\frac{\mathrm{Re}(C)}{(A+|B|)^{1/2}}\right). \tag{4.5}$$

H_j is the Hermite polynomial of order j and $f_k(A,B)$ is given by

$$f_k(A,B) = \frac{1}{k!(1-k)!}\left(\frac{A-B}{A+B}\right)^k. \tag{4.6}$$

A, B are given by

$$\begin{aligned} A(\overline{n},r) &= \overline{n}(\overline{n}+1)/\left[\overline{n}^2+(\overline{n}+1/2)(1+\cosh 2r)\right] \\ B(\overline{n},r) &= (\overline{n}+1/2)\sinh 2r/\left[\overline{n}^2+(\overline{n}+1/2)(1+\cosh 2r)\right] \end{aligned} \tag{4.7}$$

and C is given by

$$\begin{aligned} &C(\overline{n},r,\varphi) = \\ &|\alpha|(e^{\frac{i\varphi}{2}}\cosh r + e^{\frac{-i\varphi}{2}}\sinh r)\left[\frac{1}{2}+(\overline{n}+1/2)\cosh 2r\right] - \\ &|\alpha|(e^{\frac{-i\varphi}{2}}\cosh r + e^{\frac{i\varphi}{2}}\sinh r)\left[(\overline{n}+1/2)\sinh 2r\right]. \end{aligned} \tag{4.8}$$

Now that the probability function is known, the fitting model can be built. We use here the same model used in the previous chapter, that is the weighted least squares estimator with weights calculated by using the Bayes model. The data is a vector of relative frequency of brights observed $\{f_i\}$ for different pulse duration times. The weighted sum of squared residuals now is written as

$$\Delta(|\alpha|,r,\bar{n},\varphi,\Omega,\gamma|\{f_i\}) = \sum_{i=0}^{n_t} w_i\left[P_{\downarrow}(t_i||\alpha|,r,\bar{n},\varphi,\Omega,\gamma) - f_i\right]^2. \tag{4.9}$$

Now the sum is over the pulse durations t_i and n_t is the maximum pulse duration considered. The set of estimates is obtained from minimizing $\Delta(|\alpha|,r,\bar{n},\varphi,\Omega,\gamma)$. The fitting algorithm is different from the one used in the previous chapter. Now the model function is more complex and depends on more variables. It results in an estimator more sensitive to the starting conditions. To overcome this difficulty it is set a fitting process in 2 steps. The first one is set to minimize Eq. (4.9) using a global optimization method to obtain a good set of starting points. The second step is set to minimize the sum of squared residuals using a local optimization method, with the estimates obtained in the previous step as starting points.

The simulated data used in this analysis is obtained in the following way. The true values of the experiment are initially set such as the number of repetitions N, the parameters associated to the quantum state of the ion $|\alpha_T|$, r_T, $\bar{n}_T$ and φ_T, and the parameters associated to the experiment Ω and γ. The size of the Fock population of the state considered is fixed allowing one to simulate a vector of datapoints $\{f_i\}$, with $f_i = \text{Random}\left(\text{Binomial}(P_{\downarrow}(t_i||\alpha|,r,\bar{n},\varphi,\Omega,\gamma),N)\right)/N$. Examples of simulated data can be seen in Figs. 9 and 10, with plots for a thermal state and a squeezed displaced thermal state. Each figure presents two plots, one with a simulated dataset together with the $P_{\downarrow}(t)$ for a set of true values and one with the Fock population associated to the state considered.

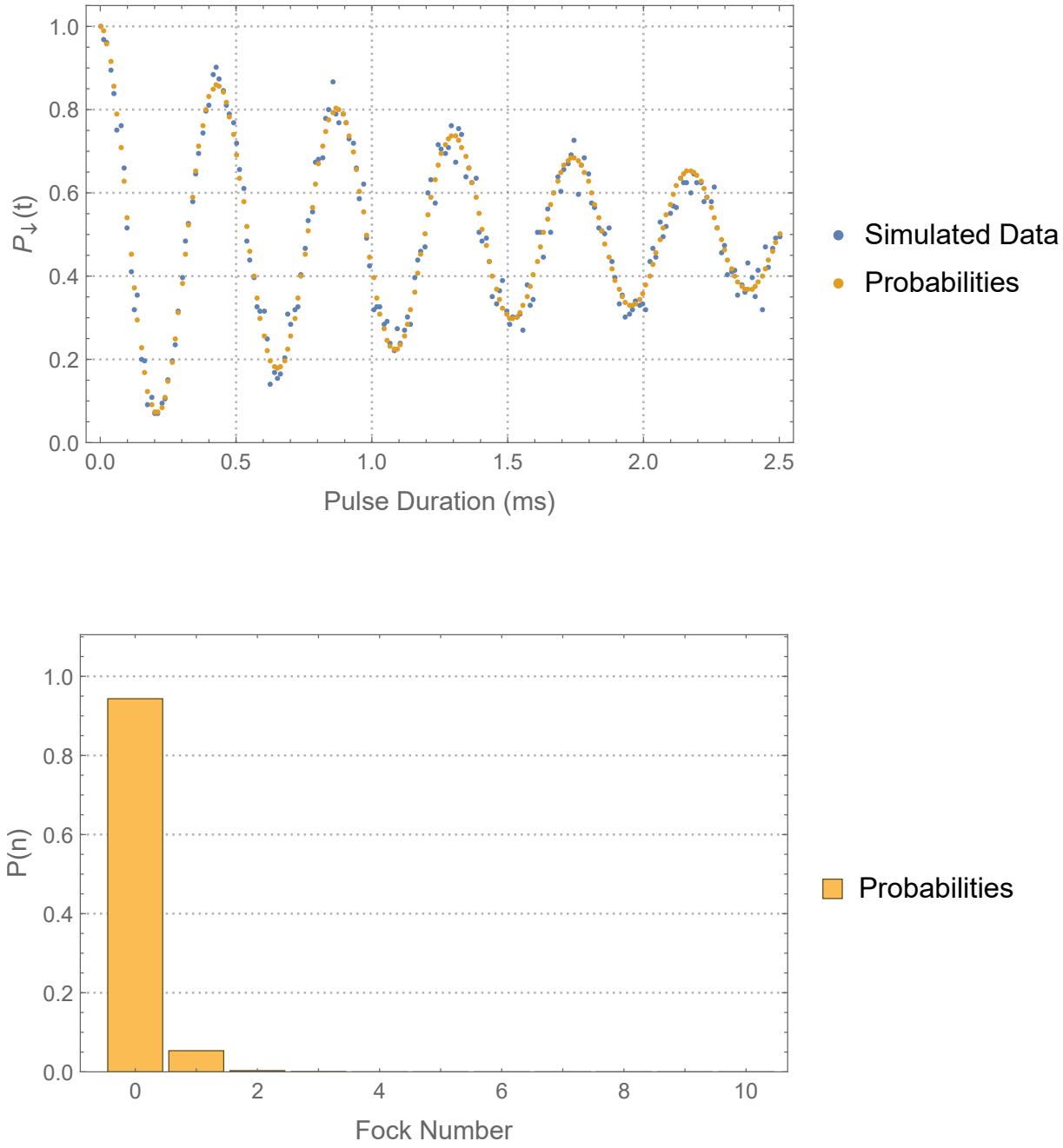

Figure 9 – The plot above presents a simulated dataset for fluorescence measurements of a single trapped ion in a thermal state and the probabilities associated to the true values of the state. Below, the probabilities $P(n)$ of the motional state chosen. The mean Fock number is $\bar{n} = 0.06$, $\Omega = 14.451$ and $\gamma = 0.51$. The number of repetitions was set to $N = 200$ for each of the 200 pulse durations.

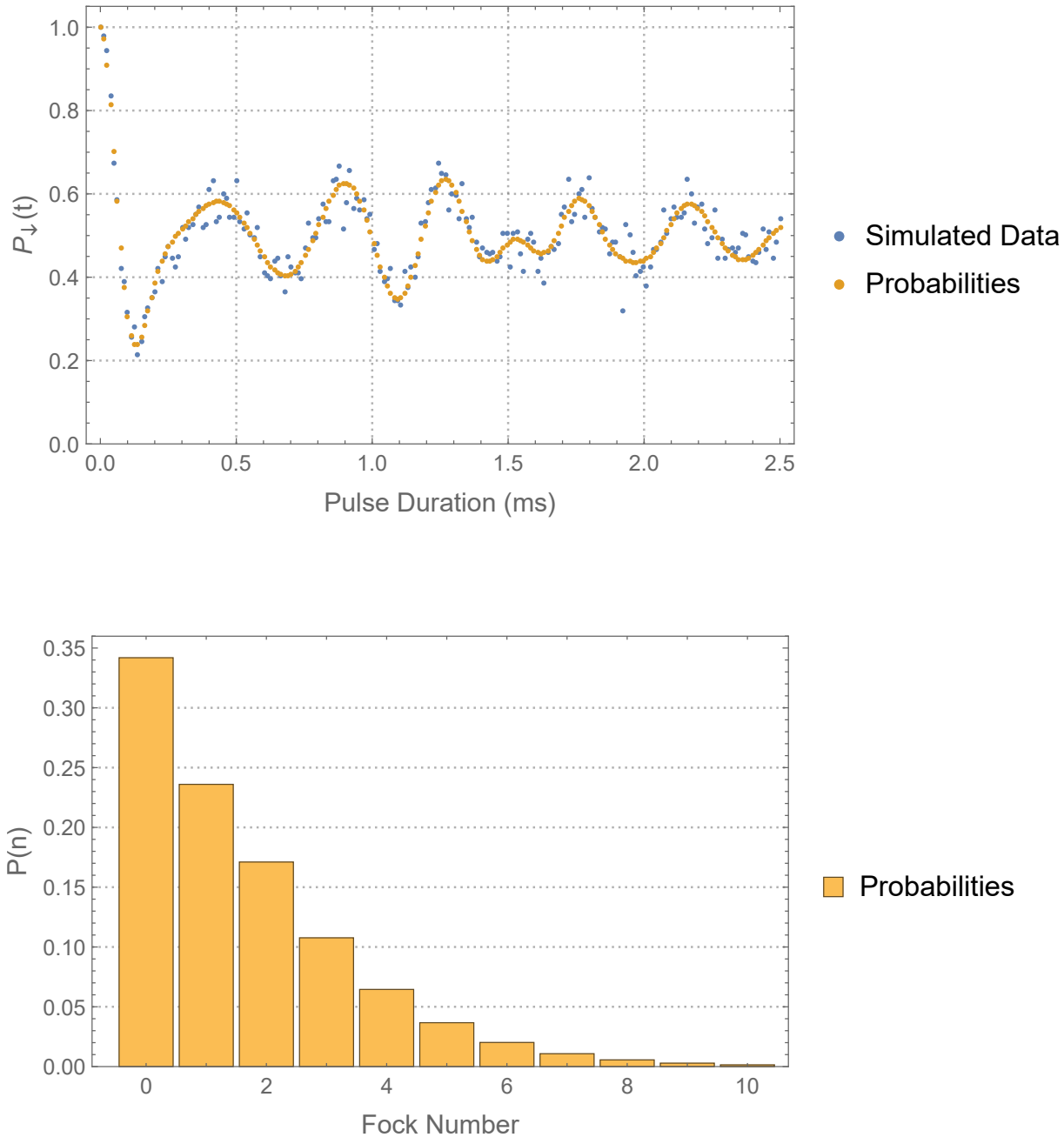

Figure 10 – The plot above presents a simulated dataset for fluorescence measurements of a single trapped ion in a squeezed displaced thermal state and the probabilities associated to the true values of the state. Below, the probabilities $P(n)$ of the motional state chosen. The true values for these plots are $|\alpha| = 0.9$, $r = 0.3$, $\bar{n} = 0.06$, $\varphi = 0$, $\Omega = 14.451$ and $\gamma = 0.51$. The number of repetitions was set to $N = 200$ for each of the 200 pulse durations.

In order to produce the final quantum state, the ion is cooled down to its initial state $\hat{\rho}_{th}$, a thermal state. It is then measured and fitted to obtain estimates for $\bar{n}$, Ω and γ. This step is called calibration step. By analysing this data we are able to learn about the final temperature of the cooling process and about the experiment parameters. The estimates obtained for Ω and γ are now used as input data to our model resulting in a reduction of the number of parameters to be estimated from six to four. Considering that those estimates are Ω_C and γ_C, the weighted sum of squared residuals for the final state can be written as

$$\Delta(|\alpha|, r, \bar{n}, \varphi|\Omega_C, \gamma_C, \{f_i\}) = \sum_{i=0}^{n_t} w_i \left[P_{\downarrow}(t_i||\alpha|, r, \bar{n}, \varphi, \Omega_C, \gamma_C) - f_i\right]^2, \tag{4.10}$$

and the same can be done to or any other state obtained from the initial state.

To be able to evaluate our model we calculate confidence intervals with bias correction, using the same method used in the previous chapter, for all set of estimates in all the simulations considered by using the same method used in the previous chapter, the parametric bootstrap method. So, given a dataset for the calibration step $\{f_i\}_{thermal}$, a set of estimates $\{\hat{n}_C, \Omega_C, \gamma_C\}$ can be obtained by

$$\{\hat{n}_C, \Omega_C, \gamma_C\} = \text{Min}[\Delta(0, 0, \bar{n}, 0, \Omega, \gamma|\{f_i\}_{thermal})]. \tag{4.11}$$

Then the estimates $\{\hat{n}_C, \Omega_C, \gamma_C\}$ are used to simulate N_{BS} bootstrap experiments obtaining the same number of datasets $\{f_{BS}\}$. The set of bootstrap estimates for the calibration step is then obtained by doing

$$\{\hat{n}_{BS}, \Omega_{BS}, \gamma_{BS}\} = \text{Min}[\Delta(0, 0, \bar{n}, 0, \Omega, \gamma|\{f_{BS}\}] \tag{4.12}$$

for all bootstrap datasets. The same procedure can be used to generate bootstrap estimates for the final state. Now, given a dataset for a final state f_F the set of estimates can be obtained by

$$\{|\alpha|_F, r_F, \bar{n}_F, \varphi_F\} = \text{Min}[\Delta(|\alpha|, r, \bar{n}, \varphi|\Omega_C, \gamma_C, \{f_F\})]. \tag{4.13}$$

The simulated bootstrap (BS) datasets for the final state $\{f_F\}_{BS}$ are then obtained by using the $\{|\alpha|_F, r_F, \bar{n}_F, \varphi_F\}$ as input parameters in the simulation procedure together with Ω_{BS} and γ_{BS}. Each simulated dataset now corresponds to a pair of bootstrap estimates for $\{\Omega_{BS}, \gamma_{BS}\}$ in order to associate each final state simulated BS experiment with a BS simulated initial state. Finally, the set of bootstrap estimates needed to calculate the confidence intervals for $\{|\alpha|_F, r_F, \bar{n}_F, \varphi_F\}$ are obtained by doing

$$\{|\alpha|_{FBS}, r_{FBS}, \bar{n}_{FBS}, \varphi_{FBS}\} = \text{Min}[\Delta(|\alpha|, r, \bar{n}, \varphi|\Omega_{BS}, \gamma_{BS}, \{f_F\}_{BS})]. \tag{4.14}$$

Repetitions	$\bar{n}$	Ω	γ
$N = 200$	{0.16, 0.21}	{14.43, 14.48}	{0.50, 0.55}
$N = 1{,}000$	{0.20, 0.22}	{14.43, 14.45}	{0.50, 0.52}
$N = 10{,}000$	{0.20, 0.20 }	{14.45, 14.45}	{0.53, 0.53}

Table 4 – Table of confidence intervals for different number of repetitions for true values equal to $\{\bar{n}, \Omega, \gamma\} = \{0.2, 14.451, 0.51\}$.

The parameters chosen to simulate the experiments to be used to test our method are based on the experiments described in (Burd *et al.* 2019) and (Burd *et al.* 2023). The next two sections present results for simulated data for different parameters considered for both calibration step and final state. First we present results for fitting the datasets to the final state individually, and then when the fit is done by joint fitting a set of datasets obtained by varying the relative phases. In the last section of the chapter, the method is applied to real data obtained in (Burd *et al.* 2023).

4.1 Individual Fitting

In this section we present results for fitting simulated data for the calibration step and two final states that differ only by the relative phase. The data analysis is based on the estimates obtained and the confidence intervals calculated.

The set of parameters chosen are $\{\bar{n}, \Omega, \gamma\} = \{0.2, 14.451(\Omega/(2\pi) = 2.3\,\text{kHz}), 0.51\}$ for calibration step, and $\{|\alpha|, r, \bar{n}, \varphi\} = \{0.9, 0.3, 0.2, \{0, \pi/2\}\}$ for the final state. The pulse duration vector has values in a range of $[0, 2.5]$ ms with $\Delta t = 0.0125$ ms. The values of φ chosen to be $\{0, \pi/2\}$ are those that provide the worst and best results respectively. $N_{BS} = 1{,}000$ and the confidence level is set to 90%. The number of repetitions is set to $N = \{200;\ 1{,}000;\ 10{,}000\}$.

The results for the calibration step can be observed at Table 4. The bigger the number of repetitions the smaller the confidence interval. $N = 10{,}000$ is big enough for the confidence interval to be as small as the true values. Table 5 presents the results for final states fit for the two different relative phases chosen. Phase $\pi/2$ presents the best overall results as can be seen by the size of the confidence intervals as the number of repetitions increases, specially for α and $\bar{n}$.

4.2 Joint Fitting

In this section we present the results for joint fitting a set of datasets obtained for different relative phases. This strategy aims to take advantage of a larger amount of data from

φ, N	$\lvert\alpha\rvert$	r	$\bar{n}$	φ
$\varphi = 0, N = 200$	{0.83, 0.99}	{0.33, 0.63}	{0.0, 0.81}	{0.0, 2.53}
$\varphi = 0, N = 1{,}000$	{0.86, 0.95}	{0, 0.3}	{0.0, 0.98}	{0.0, 0.94}
$\varphi = 0, N = 10{,}000$	{0.86, 0.90 }	{0.30, 0.46}	{0.0, 0.20}	{0.0, 0.90}
$\varphi = \pi/2, N = 200$	{0.77, 0.93}	{0.0, 0.47}	{0.0, 0.53}	{0.0, 1.85}
$\varphi = \pi/2, N = 1{,}000$	{0.86, 0.92}	{0.27, 0.44}	{0.0, 0.43}	{1.17, 1.73}
$\varphi = \pi/2, N = 10{,}000$	{0.89, 0.91 }	{0.28, 0.34}	{0.08, 0.29}	{1.43, 1.75}

Table 5 – Table of confidence intervals for different number of repetitions for a SDTS with relative phases for true values equal to $\{|\alpha|, r, \bar{n}, \varphi\} = \{0.9, 0.3, 0.2, \{0, \pi/2\}\}$.

different datasets. We assume a total number of repetitions N and that the relative phase can be changed to m known values, where $j = 1, ..., m$. We also consider that the same fraction of N/m repetitions is associated to each β_j and that k_{ij} is the number of detections for t_i and a given relative phase β_j, so that $k_{ij}/(N/m) \approx P_{\downarrow}(t_i|\beta_j)$. There is now an offset δ associated to the experiment and it is considered fixed for all datasets. Since the relative phase can be controlled, we can write $\varphi_j = \beta_j + \delta$ for $j = 1, \ldots, m$ where δ is the unknown parameter. So there are $3m+1$ parameters to be estimated since there is a set of $\{|\alpha_j|, r_j, \bar{n}_j\}$ for each β_j plus the fixed offset.

We consider here a scenario where changing the phase does not change significantly the other parameters, which means that $\{|\alpha|, r, \bar{n}\}$ are set to be the same for all datasets. As a consequence, the number of parameters to be estimated is reduced to four, $\{|\alpha|, r, \bar{n}, \delta\}$.

Now the function Δ needs to be rewritten in order to consider all data f_{ij} and weights w_{ij} for $i = 0, ..., n_t$ and $j = 1, ..., m$. Thus,

$$\Delta(|\alpha|, r, \bar{n}, \delta|\varphi_j, \Omega, \gamma, \{f_{ij}\}) = \sum_{i=0}^{n_t} \sum_{j=1}^{m} w_{ij} \left[P_{\downarrow}(t_i||\alpha|, r, \bar{n}, \varphi_j + \delta, \Omega, \gamma) - f_{ij}\right]^2. \tag{4.15}$$

Three different sets of parameters $\{|\alpha|, r, \bar{n}\}$ are considered for the same set of relative phases. They are referred to as state 1, state 2 and state 3. All three are analysed for 2 different total number of repetitions N. It will provide information about how the joint fitting performs when compared to individual fitting when the number of repetitions for each dataset is the same. Also, we take N/m smaller to check how joint fitting improves the results even if we are using less data.

The parameters for the calibration step are almost the same as in the previous section except for temperature. The set of parameters chosen are $\{\bar{n}, \Omega, \gamma\} = \{0.1, 14.451(\Omega/(2\pi) = 2.3$ kHz), $0.51\}$ and $N = 200$. The pulse duration vector has values in the range $[0, 2.5]$ ms with $\Delta t = 0.0125$ ms. The values of φ_j are $2\pi \times \{0, 0.1, 0.2, 0.3, 0.4, 0.5, 0.6, 0.7, 0.8, 0.9\}$. $N_{BS} =$

	$\bar{n}$	Ω	γ
Estimates	0.093	14.450	0.513
Conf. Intervals	{0.08, 0.12}	{14.43, 14.48}	{0.50, 0.55}

Table 6 – Point estimates and confidence intervals for calibration step used in the joint fitting results.

φ	$\lvert\alpha\rvert$	r	$\hat{n}$	φ
0	{0.96, 1.08}	{0, 0.30}	{0, 0.33}	{0, 2.27}
$2\pi\times0.1$	{0.95, 1.09}	{0, 0.35}	{0, 0.27}	{0., 2.48}
$2\pi\times0.2$	{0.92, 1.00}	{0. 0.08}	{0, 0.24}	{2.11, 3.14}
$2\pi\times0.3$	{0.91, 0.98}	{0, 0.06}	{0, 0.25}	{1.83, 3.14}
$2\pi\times0.4$	{0.93, 1.02}	{0, 0.23}	{0, 0.27}	{0, 1.93}
$2\pi\times0.5$	{0.93, 0.98}	{0, 0.34}	{0, 0.09}	{0, 1.7}
$2\pi\times0.6$	{1.06, 1.24}	{0, 0.40}	{0.21, 0.56}	{3.14, 3.14}
$2\pi\times0.7$	{0.98, 1.13}	{0, 0.32}	{0, 0.50}	{0, 0.17}
$2\pi\times0.8$	{0.98, 1.16}	{0, 0.31}	{0, 0.50}	{0.44, 3.14}
$2\pi\times0.9$	{0.94, 1.07}	{0, 0.34}	{0, 0.58}	{0, 0.12}

Table 7 – Individual fit of a set of 10 datasets for a squeezed displaced thermal state. The true values are those for state 1, with $\{|\alpha|, r, \bar{n}\}$={1.0, 0.1, 0.1}. The confidence intervals presents a confidence level of 90%. The number of repetitions was set to $N = 300$.

	$\lvert\alpha\rvert$	r	$\bar{n}$	δ
***N* = 300**				
Estimates	0.978	0.125	0.014	2.452
Conf. Intervals	{0.976, 1.002}	{0.089, 0.17}	{0.011, 0.066}	{2.121, 2.876}
***N* = 3,000**				
Estimates	0.0998	0.102	0.077	1.591
Conf. Intervals	{0.99, 0.101}	{0.09, 0.12}	{0.06, 0.11}	{1.42, 1.74}

Table 8 – Table of estimates and confidence intervals for state 1 and two different numbers of total repetitions. Each dataset was simulated with $N/10$ repetitions. The true values are $\{|\alpha|$, r, $\bar{n}\}$={1.0, 0.1, 0.1}.

1,000 and the confidence level is set to 90%. State 1 = $\{|\alpha| = 1.0, r = 0.1, \bar{n} = 0.1\}$, State 2 = $\{|\alpha| = 1.0, r = 0.02, \bar{n} = 0.1\}$ and State 3 = $\{|\alpha| = 0.5, r = 1.3, \bar{n} = 0.1\}$. For all three states the two values of N are set to be $N = \{300; 3{,}000\}$ that provides a number $N/m = \{30, 300\}$, respectively.

The values for the calibration step are presented in the table 6. Table 7 presents confidence intervals for each simulated dataset used for state 1 when fitted individually. Although most confidence intervals for the amplitude are small when compared with the true value $|\alpha| = 1.0$, there are a lot of uncertainty associated to the estimates of squeezing and temperature and relative phase. On the other hand, in Table 8 we see a lot less uncertainty in the estimates of r, $\bar{n}$ and φ for the same number of repetitions for each dataset.

	$\|\alpha\|$	r	$\bar{n}$	δ
$N = 300$				
Estimates	0.987	-0.013	0.051	3.169
Conf. Intervals	{0.980, 1.014}	{0.0, 0.015}	{0.049, 0.119}	{0.472, 5.648}
$N = 3{,}000$				
Estimates	1.002	0.017	0.089	1.630
Conf. Intervals	{0.996, 1.012}	{0.004, 0.029}	{0.076, 0.115}	{0.633, 2.702}

Table 9 – Table of estimates and confidence intervals for state 2 and two different numbers of total repetitions. Each dataset was simulated with $N/10$ repetitions. The true values are $\{|\alpha|, \text{r}, \bar{n}\}$={1.0, 0.02, 0.1}.

	$\|\alpha\|$	r	$\bar{n}$	δ
$N = 300$				
Estimates	0.494	1.283	0.052	0.167
Conf. Intervals	{0.0, 0.568}	{1.248., 1.417}	{0.0, 0.383}	{0.0, 0.390}
$N = 3{,}000$				
Estimates	0.490	1.278	0.118	2.848
Conf. Intervals	{0.463, 0.510}	{1.253, 1.317}	{0.084, 0.167}	{2.745, 2.968}

Table 10 – Table of estimates and confidence intervals for state 3 and two different numbers of total repetitions. Each dataset was simulated with $N/10$ repetitions. The true values are $\{|\alpha|, \text{r}, \bar{n}\}$={0.5, 1.3, 0.1}.

Tables 9 and 10 present results for joint fitting for different parameters. The first table refers to a state with less squeezing, which can be associated to a squeezed displaced thermal state obtained from small amount of squeezing applied or a residual squeezing as a result of an imperfect reverse squeezing protocol. Both total number of repetitions present reasonable results, specially the one with bigger N. Table 10 presents the results for a highly squeezed state with less amplitude and same temperature. These states can be associated to squeezed displaced thermal states before reverse squeezing being applied. The smaller the displacement, the bigger the uncertainty associated to it. However, even for $N = 300$ we can obtain good point estimates and very small confidence interval for r.

4.3 Experiment Data Analysis

In this section we apply our SDTS estimator to real data obtained from a single trapped ion experiment (Burd *et al.* 2023). The data available includes calibration measurements from the thermal state, data from squeezed states obtained after applying squeezing and after reversing the squeezing to check the amount of squeezing applied and the amount of residual squeezing present, respectively. It also includes displaced thermal states data, before applying

squeezing and reversing it. All datasets come together with the pulse duration vector used in the experiment.

The experiment aims to detect phase dependent amplification of the ion's motional state by detecting the ratio $|\alpha_f|/|\alpha_i|$ before squeezing ($|\alpha_i|$) and after reversing the squeezing ($|\alpha_f|$). To do that, several measurements are obtained for different relative phases and a fixed total number of repetitions in a similar way presented in the previous section. The relative phases are considered known. Since the objective is to detect $|\alpha_f|/|\alpha_i|$ dependence on the relative phase, joint fitting data must consider now all the $|\alpha|$ for each dataset as a parameter to be fitted. So, for N_{ph} phases there will be $N_{ph}+3$ parameters to be estimated: $|\alpha_k|$ (for $k = 1,...N_{ph}$), r, $\bar{n}$ and δ.

The analysis begins with the initial state. We focus here in the calibration state and squeezed thermal state analysis using both least squares (LSE) and maximum likelihood estimators (MLE). The reason for this choice will be clear in the next pages.

Before moving forward let's introduce the maximum likelihood estimator. For a single pulse duration t_i, the probability of observing a K_i number of brights over a total of N repetitions can be modeled by a binomial distribution $p_i\left[K_i|N,P_\downarrow(t_i)\right] = \text{Binomial}\left[K_i|N,P_\downarrow(t_i)\right]$. The likelihood l_i is then given by $l_i = p\left[P_\downarrow(t_i)|K_i,N\right]$. consequently, the likelihood of measuring K_i brights for a set of different pulse durations t_i is given by

$$l\left(P_\downarrow(t_i)|N,K_i\right) = \prod_{i=1}^{n_t} p_i\left[P_\downarrow(t_i)|K_i,N\right] \tag{4.16}$$

and its log-likelihood function is given by

$$\begin{aligned}
\mathbf{L}(P_\downarrow(t_i)|N,K_i) &= \log[p_i] \\
&= \log\left[\prod_{i=1}^{n_t}\binom{N}{K_i} P_\downarrow(t_i)^{K_i}\left[1-P_\downarrow(t_i)\right]^{N-K_i}\right] \\
&= \sum_{i=1}^{n_t}\left[\log\left[\binom{N}{K_i}\right] + \log\left[P_\downarrow(t_i)^{K_i}\right] + \log\left[(1-P_\downarrow(t_i))^{N-K_i}\right]\right] \\
&= \sum_{i=1}^{n_t}\left[\log\left[\binom{N}{K_i}\right] + K_i\log\left[P_\downarrow(t_i)\right] + (N-K_i)\log\left[1-P_\downarrow(t_i)\right]\right]
\end{aligned} \tag{4.17}$$

that dividing by N results in

$$\mathbf{L}(P_\downarrow(t_i)|N,K_i)/N = \sum_{i=1}^{n_t}\left[\frac{1}{N}\left[\binom{N}{K_i}\right] + f_i\log\left[P_\downarrow\right] + (1-f_i)\log\left[1-P_\downarrow(t_i)\right]\right]. \tag{4.18}$$

Considering that the objective is to maximize Eq. (4.18), the first sum can be disconsidered and

	$\bar{n}$	Ω	γ
LSE			
Estimates	0.060	14.491	0.549
Conf. Intervals	{0.046, 0.085}	{14.469, 14.513}	{0.529, 0.581}
MLE			
Estimates	0.094	14.489	0.540
Conf. Intervals	{0.070, 0.113}	{14.469, 14.514}	{0.518, 0.572}

Table 11 – Point estimates and confidence intervals for calibration step using LSE and MLE.

	$\bar{r}$	$\bar{n}$
LSE		
STS 1		
Estimates	1.261	0.172
Conf. Intervals	{1.16, 1.40}	{0.04, 0.28}
STS 2		
Estimates	0.121	0.087
Conf. Intervals	{0, 0.25}	{0.07, 0.11}
MLE		
STS 1		
Estimates	1.309	0.163
Conf. Intervals	{1.19, 1.44}	{0.03,0.29}
STS 2		
Estimates	0.352	0.073
Conf. Intervals	{0.29, 0.42}	{0.05, 0.1}

Table 12 – Point estimates and confidence intervals for both squeezed thermal states (STS) data. Both datasets were fitted using LSE and MLE. The first state (STS1) is a squeezed thermal state obtained from squeezing the initial state (thermal state). The second one (STS2) was obtained after reversing the squeezing of STS1. The confidence level is 90%.

our log-likelihood function can be written as

$$\begin{aligned}&\mathbf{L}(|\alpha|, r, \bar{n}, \delta | N, \{f_i\}) = \\ &\sum_{i=1}^{n_t} f_i \log\left[P_{\downarrow}(t_i||\alpha|, r, \bar{n}, \delta, \Omega, \gamma)\right] + \sum_{i=1}^{n_t} (1-f_i) \log\left[1 - P_{\downarrow}(t_i||\alpha|, r, \bar{n}, \delta, \Omega, \gamma)\right].\end{aligned} \tag{4.19}$$

The set of estimates provided by the MLE are those for which $\mathbf{L}(|\alpha|, r, \bar{n}, \delta | N, K_i)$ is maximum.

Table 11 present the results of fitting the calibration step data with both estimators. They present point estimates and confidence intervals with 90% of confidence level. First thing to note is that the estimates and confidence intervals both agree for Ω and γ. However, there is a big difference between the estimates for $\bar{n}$ using both estimators. Both confidence interval results barely overlap indicating that these results disagree about which one better represents the experiment. In that case an extra analysis is needed. One hypothesis is that the MLE may be influenced by an outlier more than the LSE, since this estimator weights the sum of the squared

residuals. However, results with simulated data have not presented such disagreement between both estimators.

Table 12 presents estimates and confidence intervals obtained from fitting datasets of the two squeezed thermal states (STS) provided. The first state (STS1) is a squeezed thermal state obtained from squeezing the initial thermal state. The second one (STS2) was obtained after reversing the squeezing of the first STS. Both estimators provide good estimates and confidence intervals for squeezing in STS1. Although the temperature point estimates differ significantly from those obtained in the previous table, its confidence intervals contains all the estimates for $\bar{n}$ presented in tables 11 and 12. STS2 analysis also provides good estimates with small confidence intervals for squeezing specially for MSE. Differently from the results for STS1, the temperature estimates are closer to the thermal state values and with smaller uncertainty.

To check the disagreement presented in table 11, we fitted the data disconsidering one datapoint of the dataset per fit so that the MLE was applied to a dataset with one missing point each fit and considering only the corresponding pulse durations. The result was a set of n_t estimates for $\bar{n}$ where now the influence of a single datapoint associated to a single pulse duration can be observed. Fig. 11 presents the absolute value of the difference between the estimates of $\bar{n}$ from LSE and the estimates from MLE when a data point was disconsidered. From Table 11, that difference is 0.034. If any problem is being caused by a problematic datapoint we expect that the difference gets closer to zero.

Figure 11 shows that there is one point that when removed fixed the big gap between LSE and MLE estimates for $\bar{n}$. It is the data for pulse duration $t_1 = 0$. That datapoint is associated to the initial state at which the ion is expected to be before any BSB is applied. The log-likelihood of preparing the spin down state can be written as

$$\mathbf{L}(\bar{n},\Omega,\gamma) = K_{1\downarrow} \times \log\left[P_{\downarrow}(t_1 = 0)\right] + K_{1\uparrow} \times \log\left[P_{\uparrow}(t_j)\right] + \sum_{j=2}^{n_t} K_{j\downarrow} \times \log\left[P_{\downarrow}(t_j)\right], \tag{4.20}$$

where $K_{1\downarrow}$ and $K_{1\uparrow}$ are the number of times spin down and spin up were detected before any BSB pulse was applied. $K_{j\downarrow}$ and $K_{j\uparrow}$ are the counts observed for both down and up states for all BSB pulses of duration t_j considered. The summation only consider $P_{\downarrow}(t_j)$ terms because the BSB pulse interacts with spin down states only. Since the ion is expected to be at the spin down state at $t_1 = 0$ with probability 1, the previous equation results in

$$\mathbf{L}(\bar{n},\Omega,\gamma) = K_{1\downarrow} \times 0 + K_{1\uparrow} \times (-\infty) + \sum_{j=2}^{n_t} K_{j\downarrow} \times \log\left[P_{\downarrow}(t_j)\right]. \tag{4.21}$$

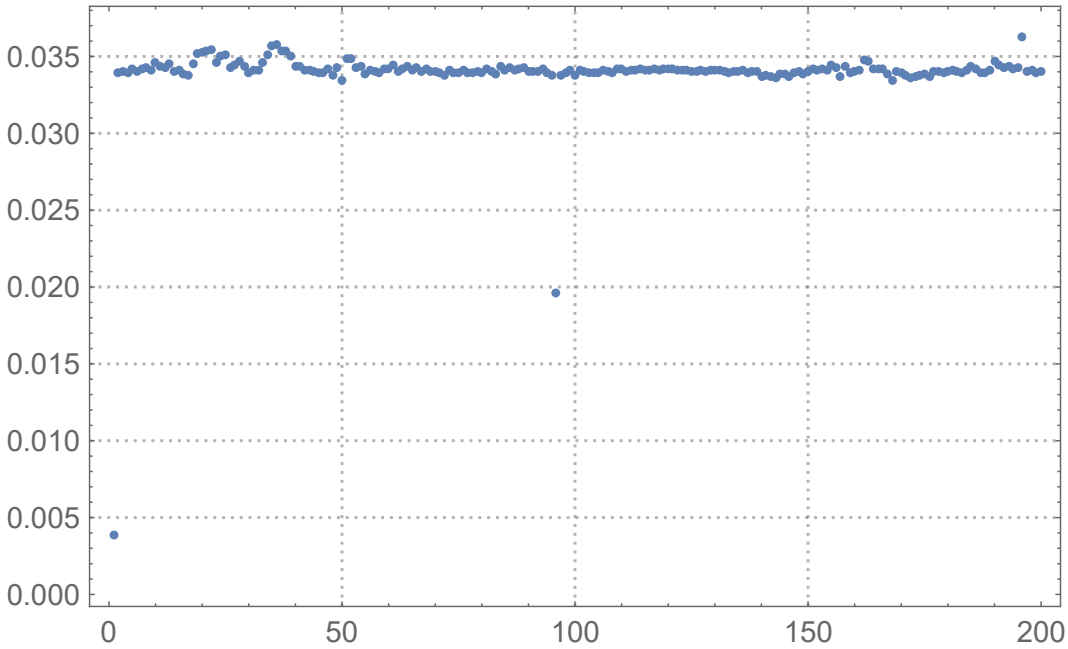

Figure 11 – $|\bar{n}_{MLE}$ - $\bar{n}_{LSE}|$ as a function of pulse duration. $\bar{n}_{MLE}$ was obtained using MLE and disconsidering one pulse duration at a time and $\bar{n}_{LSE}$ was obtained using LSE and all data points.

Since our objective is to obtain the set of estimates that maximizes Eq. (4.21), the $-\infty$ term can be disconsidered and we write

$$\begin{aligned} \text{Max}\left[\mathbf{L}(\bar{n},\Omega,\gamma)\right] &= \text{Max}\left[K_{1\downarrow}\times 0 + K_{1\uparrow}\times(-\infty) + \sum_{j=2}^{n_t} K_{j\downarrow}\times\log\left[P_{\downarrow}(t_j)\right]\right] \\ &= \text{Max}\left[\sum_{j=2}^{n_t} K_{j\downarrow}\times\log\left[P_{\downarrow}(t_j)\right]\right]. \end{aligned} \tag{4.22}$$

This tells us that we can completely ignore $t_1 = 0$ data when trying to maximize the log-likelihood function. That conclusion agrees with the results shown in Fig. 11, since it has no effect on the location of the maximum likelihood point. For pulse duration $t = 0$, the probability of measuring the spin down state is given by $P_{\downarrow}(t=0) = 1/2 + \sum_{n=0}^{\infty} P(n)/2$, and that must be 1. Since we set a size for the Fock population, that truncation may result in $\sum_{n=0}^{n_{max}} P(n) < 1$ and, consequently, $P_{\downarrow}(t=0)$ will depend on $\bar{n}$ and have some influence in the final result. This explain why considering $P_{\downarrow}(t=0)$ gives unexpected results.

According to the model, the probability of detecting a spin down state for $t = 0$ is 100%. However, the dataset provided presents $f_1 = 0.99$. That difference may be associated to some experimental error source. We present here two modifications to the model given by Eq. (4.2) that fits the requirement $P_{\downarrow}(t=0) < 1$. The first one considers a decay parameter in the exponential $e^{-\gamma_n t}$, which implies a dependence of the error source on the Fock population. The second one considers that $P_{\downarrow}(t=0)$ takes the form $P_{\downarrow}(t=0) = B/2 + A\sum_{n=0}^{\infty} P(n)/2$, where A

and B are associated to probabilities of the spin flipping from down to up and from up to down, decreasing the probability of detecting the spin down state. A particular case where $B = 0$ is considered, resulting in a total of three models analysed in the next subsections.

The analysis consists on the comparison of the mean and mean squared error (MSE) of the estimates obtained from fitting the same set of simulated datasets using LSE and MLE. Each estimator consider all proposed models. The smaller the bias presented by one model the better it describes the experiment. The estimators based on the Std model provides the reference estimates needed to the analysis. The direct comparison between Std results and the proposed model results indicates which one is more adequate. We simulate 100 experiments for each of the proposed model and fit each set with both LSE and MLE using Std model and at least one of the proposed models.

4.3.1 t_0 *Model*

The model proposed in this subsection is given by the equation

$$P_{\downarrow}(t) = \frac{1}{2} + \frac{1}{2}\sum_{n=0}^{\infty} P(n)e^{-\gamma_n(t+t_0)}\cos\Omega_n t, \tag{4.23}$$

where the parameter that models the error source in the experiment is t_0. For pulse duration $t = 0$ the probability function becomes $P_{\downarrow}(0) = \frac{1}{2} + \frac{1}{2}\sum_{n=0}^{\infty} P(n)e^{-\gamma_n t_0}$.

To test this model we consider an initial state with true parameters $\bar{n}_{true} = 0.060$, $\Omega_{true} = 14.491$ and $\gamma_{true} = 0.549$, that are the point estimates presented in Table 11. For the true value of t_0 we consider the result of the solution of the equation $0.99041 = \frac{1}{2} + \frac{1}{2}\sum_{n=0}^{\infty} P(n|\bar{n})e^{-\gamma_n t_0}$ for t_0, where 0.99041 is the measurement data for $t = 0$ for the calibration step and $P(n|\bar{n})$ is the probability function of finding the thermal state with average Fock number $\bar{n}$. The result provides $t_0 = 0.0357$. Thus, all the true values considered in the simulations are $\{\bar{n}_{true}, t_{0true}, \Omega_{true}, \gamma_{true}\} = \{0.060, 0.0357, 14.491, 0.549\}$.

The results can be found in Table 13 for estimators based on the standard model and on Eq. (4.23). The results for t_0 model estimators presents almost no bias. On the other hand, both LSE and MLE present bias similar to the standard deviation when fitting data considering the standard model, showing a consistent error associated to fitting data from a more restricted model.

However, depending on the experiment, the error source may be associated to spin flip in the state preparation instead of changes in the Fock population. In this case it is physically

	$\bar{n}$	Ω	γ	t_0
LSE				
Std Model				
Mean	0.067	14.492	0.552	
MSE	0.00021	0.00024	0.00029	-
t_0 **Model**				
Mean	0.061	14.492	0.545	0.024
MSE	0.00019	0.00035	0.00024	0.00032
MLE				
Std Model				
Mean	0.071	14.492	0.557	-
MSE	0.00028	0.00024	0.00035	-
t_0 **Model**				
Mean	0.063	14.492	0.548	0.033
MSE	0.00020	0.00024	0.00031	0.00029

Table 13 – Results for simulated data considering t_0 model fitted using LSE and MLE. Both estimators consider the standard model (Std) and A model for $P_{\downarrow}(t)$. The true values are $\{\bar{n}_{true}, t_{0true}, \Omega_{true}, \gamma_{true}\} = \{0.060, 0.0357, 14.491, 0.549\}$.

incompatible the use of the t_0 model and a new one is needed.

4.3.2 p_1p_2 *Model*

Let us consider that when preparing the ion in the spin down state there is a probability p_1 of the spin down state to flip to up. On the other hand, when the preparation results in a spin up state there is also a probability p_2 of that state flipping to down. Thus, the probability of preparing the state with spin down, that we represent by $P_{|\downarrow\rangle}$, is given by

$$\begin{aligned} P_{|\downarrow\rangle} &= (1-p_1)P_{\downarrow}(t) + p_2 P_{\uparrow}(t) \\ &= (1-p_1)P_{\downarrow}(t) + p_2\,(1-P_{\downarrow}(t)) \\ &= P_{\downarrow}(t) - p_1 P_{\downarrow}(t) + p_2 - p_2 P_{\downarrow}(t) \\ &= p_2 + P_{\downarrow}(t)(1-p_1-p_2), \end{aligned} \tag{4.24}$$

that depends now on the probability of measuring the ion's state when it is down, $P_{\downarrow}(t)$, and on the probability of measuring it when it is up, $P_{\uparrow}(t)$. Replacing Eq. (4.2) in the last equation, we obtain

$$\begin{aligned} P_{|\downarrow\rangle} &= p_2 + \left(\frac{1}{2} + \frac{1}{2}\sum_{i=0}^{\infty} P(n)e^{-\gamma_n t}\cos\Omega_n t\right)(1-p_1-p_2) \\ &= p_2 + \frac{(1-p_1-p_2)}{2} + \frac{(1-p_1-p_2))}{2}\sum_{i=0}^{\infty} P(n)e^{-\gamma_n t}\cos\Omega_n t \end{aligned} \tag{4.25}$$

	$\bar{n}$	Ω	γ	A
LSE				
Std Model				
Mean	0.068	14.491	0.554	-
MSE	0.00022	0.00015	0.00023	-
A Model				
Mean	0.061	14.491	0.547	0.986
MSE	0.00018	0.00011	0.00015	0.00023
MLE				
Std Model				
Mean	0.071	14.491	0.561	-
MSE	0.00037	0.00015	0.00044	-
A Model				
Mean	0.063	14.491	0.549	0.981
MSE	0.00018	0.00008	0.00015	0.00022

Table 14 – Results for simulated data considering the A model fitted using LSE and MLE. Both estimators considered the standard model (Std) and the A model for $P_{\downarrow}(t)$. The true values are $\{\bar{n}_{true}, A_{true}, \Omega_{true}, \gamma_{true}\} = \{0.060, 0.0980, 14.491, 0.549\}$.

Finally

$$P_{|\downarrow\rangle} = \frac{(1-p_1+p_2)}{2} + \frac{(1-p_1-p_2)}{2}\sum_{i=0}^{\infty} P(n)e^{-\gamma_n t}\cos\Omega_n t. \tag{4.26}$$

When $p_1 = p_2$ the model becomes

$$P_{|\downarrow\rangle} = \frac{1}{2} + \frac{A}{2}\sum_{i=0}^{\infty} P(n)e^{-\gamma_n t}\cos\Omega_n t, \tag{4.27}$$

where $A = 1 - p_1 - p_2$. It is called the A model. The most general one, given by Eq. (4.26) is referred to in our analysis as the p_1p_2 model. The procedure to test both A and p_1p_2 models is the same used to test the t_0 model.

Let us begin with the A model. Some of the true values used to simulate data are the same used in the previous section. The only change is that now there is no t_0 but A. From Eq. (4.26), for $t = 0$, we obtain that $A = 2P_{\downarrow}(0) - 1$. Using the experiment's data point for $t = 0$ as $P_{\downarrow}(0)$ $A = 0.980$, we get the true value for A that will be considered in the simulation. Therefore, the true parameters considered are $\{\bar{n}_{true}, A_{true}, \Omega_{true}, \gamma_{true}\} = \{0.060, 0.980, 14.491, 0.549\}$.

The results are presented in Table 14 for the standard model and the A model based estimators. Both estimators for the standard model present significant bias, specially for MLE, for which the bias presented is bigger than the standard deviation.

The p_1p_2 model considers different probabilities for p_1 and p_2. We guess these probabilities to be $p_1 = 2\%$ and $p_2 = 3\%$ in our test. Smaller spin flip probabilities may occur

	$\bar{n}$	Ω	γ	A	p_1	p_2
LSE						
Std Model						
Mean	0.079	14.492	0.574	-	-	-
MSE	0.00048	0.00017	0.00086	-	-	-
A Model						
Mean	0.061	14.493	0.555	0.964	-	-
MSE	0.00019	0.00018	0.00037	0.00038	-	-
p1p2 Model						
Mean	0.059	14.493	0.550	-	0.016	0.026
MSE	0.00018	0.00018	0.00034	-	0.00006	0.00007
MLE						
Std Model						
Mean	0.084	14.492	0.579	-	-	-
MSE	0.00074	0.00018	0.00114	-	-	-
A Model						
Mean	0.063	14.493	0.556	0.956	-	-
MSE	0.00019	0.00018	0.00037	0.00021	-	-
p1p2 Model						
Mean	0.060	14.493	0.551	-	0.020	0.030
MSE	0.00018	0.00018	0.00033	-	0.00004	0.00005

Table 15 – Results for simulated data considering p_1p_2 model fitted using LSE and MLE. Both estimators considered the standard model (Std), the A model and the p_1p_2 model for $P_{\downarrow}(t)$. The true values are $\{\bar{n}_{true}, p_{1_{true}}, p_{2_{true}}, \Omega_{true}, \gamma_{true}\} = \{0.060, 0.02, 0.03, 14.491, 0.549\}$.

and consequently it may be harder to distinguish between p_1 and p_2. For this simulation, the true values considered are $\{\bar{n}_{true}, p_{1_{true}}, p_{2_{true}}, \Omega_{true}, \gamma_{true}\} = \{0.060, 0.02, 0.03, 14.491, 0.549\}$. We present next the results from fitting the 100 simulated datasets considering estimators for the standard model and the p_1p_2 model. We add the results for estimators for A model in order to be able to compare how different its results are from those for p_1p_2 model.

Table 15 presents the results of the tests for p_1p_2 model. The first table presents the results for the standard model fit, the second one for A model fit and the last one for p_1p_2 fit. The best results are those for p_1p_2 model. For the standard one there is significant bias and big mean squared error compared to the other two models. The A and p_1p_2 models results differ by a small difference. The estimates for A in table 15 may be compared to $1 - p_1 - p_2 = 0.95$. Even being considered as an approximation, the A model presents close results to the more general one.

	$\bar{n}$	Ω	γ	A	p_1	p_2
LSE						
Std Model						
LSE Fit	0.06043	14.49100	0.54942	-	-	-
MLE Fit	0.06431	14.49300	0.56250	-	-	-
A Model						
LSE Fit	0.05629	14.49100	0.54461	0.99108	-	-
MLE Fit	0.05659	14.49300	0.55353	0.98343	-	-
p1p2 Model						
LSE Fit	0.04172	14.49300	0.53655	-	0.04190	$8.63340 \times 10\text{-}15$
MLE Fit	0.02733	14.49600	0.55437	-	0.05069	$1.44840 \times 10\text{-}15$

Table 16 – Estimates obtained from fitting experimental data for calibration step using least squares estimator(LSE) and maximum likelihood estimator(MLE) considering the three models tested: Std, A model and $p_1 p_2$ model.

4.3.3 Real Data Tests

In this section we apply our estimators based on each new model functions to the data. The results are presented in Table 16. Results are for fitting the data considering an estimator based on the standard model (Std), the A model and the $p_1 p_2$ model. We also have Table 17 to check if the estimates obtained are really the best for each model. Since the LSE minimizes the sum of squared residuals, the sum for its estimates must be smaller than the sum of squared residuals for the estimates obtained from MLE. In the other hand, the estimates obtained from MLE must present bigger likelihood than those obtained from LSE.

As we can see in table 16, the estimates for temperature when using the A model are smaller, but close to 0.06. There is a significant change in the estimates for Ω and γ. Estimates for $\bar{n}$ using the $p_1 p_2$ model indicates that the data provided does not allows us to obtain good estimates considering spin flip probabilities, since the values are a lot smaller and the estimates for p_2 seems unrealistic. Table 17 presents the sum of the squared residuals and the log-likelihoods for each set of estimates obtained from all the models considered. The A model and $p_1 p_2$ model estimates present smaller sum of residuals than those obtained from Std model when using LSE. On the other hand, their likelihoods are also bigger than the likelihoods for Std model estimates when using MLE.

4.3.4 Amplification Analysis

In this section we present results of individual and joint fitting datasets in order to detect amplitude amplification after squeezing and then reversing the squeezing of a displaced

	LSE Fit	MLE Fit
Squared Residuals		
Std Model	507.859	509.702
A0 Model	507.178	509.536
p1p2 Model	377.86	385.42
Likelihoods		
Std Model	-53.237	-53.2322
A0 Model	-53.1216	-53.1186
p1p2 Model	-52.9735	-52.9716

Table 17 – Weighted sum of squared residuals and likelihoods of the point estimates presented in table 16.

thermal state (DTS). It means we need to estimate the amplitude before the squeezing operations, and to estimate the amplitude of the final state. The final state is considered to be in a squeezed displaced thermal state (SDTS) because we consider some residual squeezing. It is shown in Table 12 that squeezing and reversing of squeering (STS2) results in a residual squeezing around $r = 0.3$.

It may be difficult to distinguish between displacement and temperature when fitting a SDTS depending on the displacement applied and the amount of data provided, resulting in estimates with big confidence intervals and/or unrealistic point estimates. One way to overcome it is, besides the option of fixing it with more data, fixing the value for temperature estimate. It means that there is no significant change in the temperature when the amplification protocol is applied. The results presented in this section assumes that restriction.

To do so we choose the point estimate for $\bar{n}$ presented in Table 11 for MLE, considering the standard model for the pulse duration data. The results consists on point estimates and confidence intervals obtained from fitting a DTS data and joint fitting SDTS data for a set of relative phases after the amplification protocol. In order to better identify the amplification we estimate confidence intervals for the results.

We joint fit 10 datasets for the ten different relative phases $2\pi \times \{0.1, 0.2, 0.3, 0.4, 0.5, 0.6, 0.7, 0.8, 0.9\}$. Since there are 10 relative phases, the number of parameters to be estimated when joint fitting the data is $10 + 2 = 12$; 10 amplitudes, the residual squeezing and the offset δ. The temperature is fixed. We use here MLE only, since the temperature chosen was obtained from fitting the calibration data using MLE.

The ratio $|\alpha_f|/|\alpha_i|$ depends on the amplitude point estimates before squeezing ($|\alpha_i|$) and after reversing the squeezing ($|\alpha_f|$). To obtain the first, we fit the data for the DTS obtained before squeezing it. The result is $|\alpha_i| = 0.496$ with confidence interval $\{0.48, 0.52\}$.

	Estimates	Confidence Intervals
$\|\alpha_1\|$	0.919	{0.89, 0.95}
$\|\alpha_2\|$	0.923	{0.89, 0.96}
$\|\alpha_3\|$	1.227	{1.20, 1.27}
$\|\alpha_4\|$	1.306	{1.26, 1.35}
$\|\alpha_5\|$	1.068	{1.03, 1.10}
$\|\alpha_6\|$	0.807	{0.78, 0.84}
$\|\alpha_7\|$	0.589	{0.56, 0.61}
$\|\alpha_8\|$	0.668	{0.65, 0.69}
$\|\alpha_9\|$	0.769	{0.75, 0.80}
$\|\alpha_{10}\|$	0.919	{0.89, 0.95}
r	0.582	{0.56, 0.60}
δ	1.912	{1.85, 1.97}

Table 18 – Estimates obtained from joint fitting a set of 10 datasets for different relative phases. All the datasets were obtained from measuring the ion on a SDTS after the amplification protocol. We used MLE with fixed temperature at $\bar{n} = 0.094$.

Table 18 presents the results for joint fitting the 10 datasets. All of them present small confidence intervals. Some of the estimates are more than two times the value of $|\alpha_i|$. In order to better characterize the amplification it is important to know the uncertainty associated to each value $|\alpha_f|/|\alpha_i|$. To do so we use our bias-corrected percentile method with a set of bootstrap replicates obtained from $|\alpha_{f_{BS}}|/|\alpha_{i_{BS}}|$, the ratio between the corresponding bootstrap replicates, for each relative phase. Fig. 12 presents a plot of the point estimates for the final states and its confidence interval bars. It is interesting to see that all bars are above the region defined by the confidence interval limits of the DTS state. The second plot presents the amplitude ratios and its confidence interval bars. All red points in that plot together with their bars are above one, indicating amplification for all points. It also shows the dependence of the amplification on the relative phase.

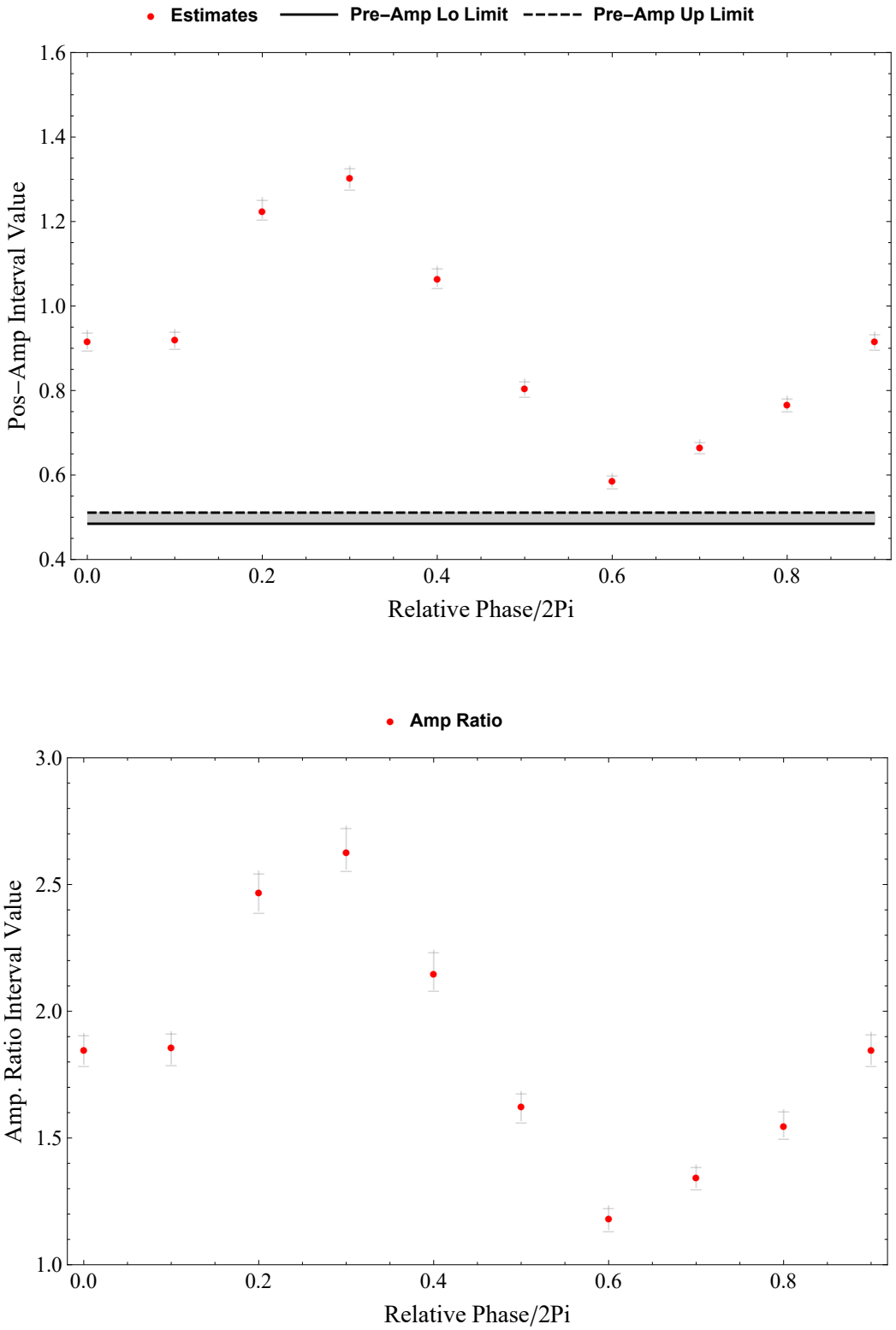

Figure 12 – Estimates of the final states for each relative phase with confidence interval bars of 1 standard deviation(above plot) and amplification ratio with confidence interval bars for 1 standard deviation(plot below) for different relative phases.

5 CONCLUSION

In this work we presented a method of inference for any single mode squeezed displaced thermal state based on the weighted least-squares and maximum likelihood estimators. The results of our tests using simulated data for a squeezed thermal state showed high fidelity results. The use of bias-correcting confidence intervals mitigates the bias present in the point estimates from smaller data sets of highly-squeezed, low temperature states. Also, when dealing with trapped ion's fluorescence measurements good estimates for displacement were obtained and joint fitting datasets with different relative phases allows better point estimates and less uncertainty associated.

These tools allow one to learn key properties of squeezed thermal states without the need for a phase reference (such as a local oscillator) in systems such as trapped ions (Burd *et al.* 2019) or integrated quantum optics (Sahin *et al.* 2013; Höpker *et al.* 2019), where performing Fock measurements is convenient. Errors related to the preparation of a trapped ion state must be considered in order to correctly estimate its motional state parameters. The analysis also presented a method to estimate amplification of an ion's motional state. As a future work we want to apply this method and the new model for pulse duration probabilities to real data obtained from a single trapped ion state. It would allow us to check the estimates for p_1 and p_2 and its uncertainty and to check how does the system's temperature behave when displacing and squeezing the initial thermal state, since we considered it fixed in the final analysis.

REFERENCES

ACERNESE, F. *et al.* Increasing the astrophysical reach of the advanced Virgo detector via the application of squeezed vacuum states of light. **Phys. Rev. Lett.**, American Physical Society, v. 123, p. 231108, Dec 2019. Available at: <https://link.aps.org/doi/10.1103/PhysRevLett.123.231108>.

AITKIN, M. **Statistical Inference**. New York: Chapman and Hall/CRC, 2010. 143–144 p. (Monographs on statistics and applied probability).

ARRAZOLA, J. M.; BERGHOLM V.AND BR´ADLER, K.; BROMLEY, T.; COLLINS, M.; DHAND, I.; FUMAGALLI, A.; GERRITS, T.; GOUSSEV, A.; HELT, L.; HUNDAL, J.; ISACSSON, T.; ISRAEL, R.; IZAAC, J.; JAHANGIRI, S.; JANIK, R.; KILLORAN, N.; KUMAR, S.; LAVOIE, J.; LITA, A.; MAHLER, D.; MENOTTI, M.; B.MORRISON; NEUHAUS, S. N. amd L.; QI, H.; QUESADA, N.; REPINGON, A.; SABAPATHY, K.; M.SCHULD; SU, D.; SWINARTON, J.; SZ´AVA, A.; TAN, K.; TAN, P.; VAIDYA, V.; VERNON, Z.; ABANEH, Z.; ZHANG, Y. Quantum circuits with many photons on a programmable nanophotonic chip. **Nature**, v. 591, n. 54, 2021. Available at: <https://doi.org/10.1038/s41586-021-03202-1>.

BURD, S. C.; KNAACK, H. M.; SRINIVAS, R.; ARENZ, C.; COLLOPY, A. L.; STEPHENSON, L. J.; WILSON, A. C.; WINELAND, D. J.; LEIBFRIED, D.; BOLLINGER, J. J.; ALLCOCK, D. T. C.; SLICHTER, D. H. Experimental speedup of quantum dynamics through squeezing. 2023.

BURD, S. C.; SRINIVAS, R.; BOLLINGER, J. J.; WILSON, A. C.; WINELAND, D. J.; LEIBFRIED, D.; SLICHTER, D. H.; ALLCOCK, D. T. C. Quantum amplification of mechanical oscillator motion. **Science**, American Association for the Advancement of Science, v. 364, n. 6446, p. 1163–1165, 2019. ISSN 0036-8075. Available at: <https://science.sciencemag.org/content/364/6446/1163>.

CARPENTER, J.; BITHELL, J. Bootstrap confidence intervals: when, which, what? a practical guide for medical statisticians. **Statistics in Medicine**, v. 19, n. 9, p. 1141–1164, 2000. Available at: <https://onlinelibrary.wiley.com/doi/pdf/10.1002/>.

DODONOV, V. V.; MAN'KO, O. V.; MAN'KO, V. I. Photon distribution for one-mode mixed light with a generic Gaussian Wigner function. **Phys. Rev. A**, American Physical Society, v. 49, p. 2993–3001, Apr 1994. Available at: <https://link.aps.org/doi/10.1103/PhysRevA.49.2993>.

EFRON, B. **The Jackknife, the Bootstrap and Other Resampling Plans**. Philadelphia: Society for Industrial and Applied Mathematics, 1982. 82–86 p.

EFRON, B.; TIBSHIRANI, R. J. **An introduction to the bootstrap**. London: Chapman and Hall, 1993. (Mono. Stat. Appl. Probab.).

FURUSAWA, A.; SØRENSEN, J. L.; BRAUNSTEIN, S. L.; FUCHS, C. A.; KIMBLE, H. J.; POLZIK, E. S. Unconditional quantum teleportation. v. 282, p. 706–709, Oct. 1998.

GOTTESMAN, D.; KITAEV, A.; PRESKILL, J. Encoding a qubit in an oscillator. **Phys. Rev. A**, American Physical Society, v. 64, p. 012310, Jun 2001. Available at: <https://link.aps.org/doi/10.1103/PhysRevA.64.012310>.

HANSEN P. C., P. V.; SCHERER, D. **Least Squares Data Fitting with Applications**. Baltimore, Maryland 21218-4363: John Hopkins University Press, 2013.

HOFHEINZ, M.; WANG, H.; ANSMANN, M.; BIALCZAK; C., R.; LUCERO, E.; NEELEY M.AND O'CONNELL, A. D.; SANK, D.; WENNER, J.; MARTINIS, J. M.; ; CLELAND, A. N. Synthesizing arbitrary quantum states in a superconducting resonator. **Nature**, v. 459, p. 546–549, 2009. ISSN 1476-4687. Available at: <https://doi.org/10.1038/nature08005>.

HöPKER, J. P.; GERRITS, T.; LITA, A.; KRAPICK, S.; HERRMANN, H.; RICKEN, R.; QUIRING, V.; MIRIN, R.; NAM, S. W.; SILBERHORN, C.; BARTLEY, T. J. Integrated transition edge sensors on titanium in-diffused lithium niobate waveguides. **APL Photonics**, v. 4, n. 5, p. 056103, 2019. Available at: <https://doi.org/10.1063/1.5086276>.

JOO, J.; MUNRO, W. J.; SPILLER, T. P. Quantum metrology with entangled coherent states. **Phys. Rev. Lett.**, American Physical Society, v. 107, p. 083601, Aug 2011. Available at: <https://link.aps.org/doi/10.1103/PhysRevLett.107.083601>.

LEIBFRIED, D.; MEEKHOF, D. M.; KING, B. E.; MONROE, C.; ITANO, W. M.; WINELAND, D. J. Experimental determination of the motional quantum state of a trapped atom. **Phys. Rev. Lett.**, American Physical Society, v. 77, p. 4281–4285, Nov 1996. Available at: <https://link.aps.org/doi/10.1103/PhysRevLett.77.4281>.

LOLLI, L.; TARALLI, E.; RAJTERI, M. Ti/Au TES to discriminate single photons. **J. Low. Temp. Phys.**, v. 167, p. 803–808, June 2012. Available at: <https://doi.org/10.1007/s10909-012-0473-2>.

LVOVSKY, A. I.; RAYMER, M. G. Continuous-variable optical quantum-state tomography. v. 81, p. 299–332, Mar. 2009.

MALLET, F.; CASTELLANOS-BELTRAN, M. A.; KU, H. S.; GLANCY, S.; KNILL, E.; IRWIN, K. D.; HILTON, G. C.; VALE, L. R.; LEHNERT, K. W. Quantum state tomography of an itinerant squeezed microwave field. **Phys. Rev. Lett.**, American Physical Society, v. 106, p. 220502, Jun 2011. Available at: <https://arxiv.org/abs/1012.0007v2>.

MARIAN, P. Higher-order squeezing and photon statistics for squeezed thermal states. **Phys. Rev. A**, American Physical Society, v. 45, p. 2044–2051, Feb 1992. Available at: <https://link.aps.org/doi/10.1103/PhysRevA.45.2044>.

MARIAN, P.; MARIAN, T. A. Squeezed states with thermal noise. ii. damping and photon counting. **Phys. Rev. A**, American Physical Society, v. 47, p. 4487–4495, May 1993. Available at: <https://link.aps.org/doi/10.1103/PhysRevA.47.4487>.

MARIAN, P.; MARIAN, T. A. Uhlmann fidelity between two-mode Gaussian states. **Phys. Rev. A**, American Physical Society, v. 86, p. 022340, Aug 2012. Available at: <https://link.aps.org/doi/10.1103/PhysRevA.86.022340>.

MEEKHOF, D. M.; MONROE, C.; KING, B. E.; ITANO, W. M.; WINELAND, D. J. Generation of nonclassical motional states of a trapped atom. **Phys. Rev. Lett.**, American Physical Society, v. 76, p. 1796–1799, Mar 1996. Available at: <https://link.aps.org/doi/10.1103/PhysRevLett.76.1796>.

MORAIS, L. A.; WEINHOLD, T.; ALMEIDA, M. P. de; LITA, A.; GERRITS, T.; NAM, S. W.; WHITE, A. G.; GILLETT, G. Precisely determining photon-number in real-time. 2020.

MYERSON, A. H.; SZWER, D. J.; WEBSTER, S. C.; ALLCOCK, D. T. C.; CURTIS, M. J.; IMREH, G.; SHERMAN, J. A.; STACEY, D. N.; STEANE, A. M.; LUCAS, D. M. High-fidelity readout of trapped-ion qubits. **Phys. Rev. Lett.**, American Physical Society, v. 100, p. 200502, May 2008. Available at: <https://link.aps.org/doi/10.1103/PhysRevLett.100.200502>.

OLIVARES, S. Quantum optics in the phase space. **Eur. Phys. J. Spec. Top.**, v. 203, p. 3–24, 2012. Available at: <https://link.springer.com/article/10.1140/epjst/e2012-01542-2>.

RAFFAELLI, F.; FERRANTI, G.; MAHLER, D. H.; SIBSON, P.; KENNARD, J. E.; SANTAMATO, A.; SINCLAIR, G.; BONNEAU, D.; THOMPSON, M. G.; MATTHEWS, J. C. F. A homodyne detector integrated onto a photonic chip for measuring quantum states and generating random numbers. **Quantum Science and Technology**, IOP Publishing, v. 3, n. 2, p. 025003, feb 2018. Available at: <https://doi.org/10.1088/2058-9565/aaa38f>.

RALPH, T. C.; GILCHRIST, A.; MILBURN, G. J.; MUNRO, W. J.; GLANCY, S. Quantum computation with optical coherent states. **Phys. Rev. A**, American Physical Society, v. 68, p. 042319, Oct 2003. Available at: <https://link.aps.org/doi/10.1103/PhysRevA.68.042319>.

ŘEHÁČEK, J.; HRADIL, Z.; KNILL, E.; LVOVSKY, A. I. Diluted maximum-likelihood algorithm for quantum tomography. **Phys. Rev. A**, American Physical Society, v. 75, p. 042108, Apr. 2007. Available at: <http://link.aps.org/doi/10.1103/PhysRevA.75.042108>.

SAHIN, D.; GAGGERO, A.; ZHOU, Z.; JAHANMIRINEJAD, S.; MATTIOLI, F.; LEONI, R.; BEETZ, J.; LERMER, M.; KAMP, M.; HöFLING, S.; FIORE, A. Waveguide photon-number-resolving detectors for quantum photonic integrated circuits. **Applied Physics Letters**, v. 103, n. 11, p. 111116, 2013. Available at: <https://doi.org/10.1063/1.4820842>.

SMITHEY, D. T.; BECK, M.; RAYMER, M. G.; FARIDANI, A. Measurement of the Wigner distribution and the density matrix of a light mode using optical homodyne tomography: Application to squeezed states and the vacuum. **Phys. Rev. Lett.**, American Physical Society, v. 70, p. 1244–1247, Mar 1993. Available at: <https://link.aps.org/doi/10.1103/PhysRevLett.70.1244>.

TSE, M. *et al.* Quantum-enhanced advanced LIGO detectors in the era of gravitational-wave astronomy. **Phys. Rev. Lett.**, American Physical Society, v. 123, p. 231107, Dec 2019. Available at: <https://link.aps.org/doi/10.1103/PhysRevLett.123.231107>.

WINELAND, D.; LEIBFRIED, D. Quantum information processing and metrology with trapped ions. **Laser Physics Letters**, IOP Publishing, v. 8, n. 3, p. 175–188, jan 2011. Available at: <https://doi.org/10.1002%2Flapl.201010125>.

APPENDIX A – *QUANTUM INFORMATION PROCESSING (2022) 21:365*

Quadrature Squeezing and Temperature Estimation from the fock Distribution.

Quantum Information Processing (2022) 21:365
https://doi.org/10.1007/s11128-022-03677-5

Quadrature squeezing and temperature estimation from the Fock distribution

Italo Pereira Bezerra[1,2] · Hilma M. Vasconcelos[2] · Scott Glancy[3]

Received: 16 March 2022 / Accepted: 9 September 2022 / Published online: 3 november 2022

Abstract

We present a method to estimate the amount of squeezing and temperature of a single-mode Gaussian harmonic oscillator state based on the weighted least-squares estimator applied to measured Fock state populations. Squeezing and temperature, or equivalently the quadrature variances, are essential parameters states used in various quantum communication and sensing protocols. They are often measured with homodyne-style detection, which requires a phase reference such as a local oscillator. Our method allows estimation without a phase reference, by using for example a photon-number-resolving detector. To evaluate the performance of our estimator, we simulated experiments with different values of squeezing and temperature. From 10,000 Fock measurement events, we produced estimates for states whose fidelities to the true state are greater than 99.99% for small squeezing ($r < 1.0$), and for high squeezing ($r = 2.5$), we obtain fidelities greater than 99.9%. We also report confidence intervals and their coverage probabilities.

Keywords Gaussian states · Squeezing · Fock population

✉ Italo Pereira Bezerra
italo@fisica.ufc.br

Hilma M. Vasconcelos
hilma@ufc.br

Scott Glancy
scott.glancy@nist.gov

[1] Universidade Estadual do Ceará, Iguatu, Ceará, Brazil

[2] Departamento de Engenharia de Teleinformática, Universidade Federal do Ceará, Fortaleza, Ceará, Brazil

[3] National Institute of Standards And Technology, Boulder, Colorado, USA